Radial velocity technique

Trifon Trifonov,a,b

aUniverstät Heidelberg, Landessternwarte, Zentrum für Astronomie, Königstuhl 12, 69117 Heidelberg, Germany
bSofia University "St. Kliment Ohridski", Department of Astronomy, Faculty of Physics, James Bourchier Blvd., BG-1164 Sofia, Bulgaria

Abstract

The precise Doppler method for measuring stellar radial velocities (RV) is a fundamental technique in modern astronomy. This method records a star's spectrum and detects periodic Doppler shifts in its spectral features, which indicate the gravitational influences induced by orbiting companions. The Doppler technique has yielded remarkable successes in exoplanet detection, uncovering a diverse array of planetary systems ranging from hot Jupiters to Neptune-mass planets and super-Earths. Having led to the discovery of over 1,100 exoplanets, the RV method is the most effective approach for measuring orbital geometries and minimum masses, which are of fundamental importance when accessing planet formation and evolution scenarios. However, exoplanet detection via precise RV measurements poses significant challenges, including managing various sources of interference, such as instrumental errors, and mitigating spurious Doppler shifts induced by phenomena like stellar activity. Key to this technique's advancement is instrumental calibration methods, notably precise calibration methods and ultra-stable spectrographs. This technique holds promise in systematically exploring the domain of Jovian analogs, rocky and icy planets within the habitable zones of their parent stars, and providing crucial follow-up observations for transiting candidates detected by space missions. The synergy between transit and Doppler measurements of exoplanets, when feasible, has provided a comprehensive set of orbital and physical parameters for exoplanets, such as the dynamical mass and mean planet density, which is of paramount importance in thereby enhancing our understanding of their internal composition. Additionally, ongoing efforts aim to improve the RV technique further by developing more stable calibration techniques aimed at detecting Earth-like analogs around Solar-type stars that require $cm\,s^{-1}$ RV precision.

Contents

Learning Objectives

This chapter aims to provide the very basic principles of the precise Doppler spectroscopy method for the detection of exoplanets around stars. By the end of this chapter, you will learn:

- History of the Doppler method in exoplanet Astronomy.
- Impact of the precise RV method of discovering exoplanets.
- Basic principles of measuring precise RVs using Échelle spectrographs.
- How to interpret and model RV data, and derive orbital parameters.
- Limitations on RVs measurements due to instrumental effects and stellar activity.
- The future role of the RV method in modern astronomy and astrophysics.

Glossary

Argument of periastron (or pericenter) in the context of exoplanets ω is the angle from the ascending node of the exoplanet's orbit to its closest point to the host star, measured in the direction of motion.

Échelle spectrograph A type of modern high-resolution spectrograph that uses a second diffraction element (grating or a prism) to disperse light into multiple orders, allowing for the simultaneous observation of a wide spectral range across many narrow bandwidths.

Eccentric anomaly in the context of exoplanets is an angular parameter that represents the position of an exoplanet along its elliptical orbit, measured from the centre of the ellipse to the projection of the planet's position onto the circumscribed circle.

Fabry–Pérot etalon is used for correcting for instrumental drifts and potentially for precise wavelength calibration in Échelle spectrographs. F-P etalons can achieve RV precision of a few $cm\,s^{-1}$ when actively controlled using atomic references.

Habitable zone is an orbital zone, which allows for temperatures just right for liquid water to exist on a planet's surface.

Inclination in the context of exoplanets, the inclination angle i refers to the angle between the plane of the planet's orbit around its host star and the line of sight from an observer on Earth.

Iodine cell is the best-known example of a gas absorption cell filled with iodine gas heated to about 50 C° and placed in the optical path of a spectrograph. The superimposed spectra of I_2 absorption lines onto the stellar spectra provide an accurate wavelength reference for precise RV measurements.

Laser Frequency Comb calibrator provides a dense array of equally spaced laser peaks over a broad bandwidth for precision and stability for wavelength calibration in Échelle spectrographs. This technology promises RV precision down to $1\,cm\,s^{-1}$.

Markov chain Monte Carlo is a computational algorithm that samples fitting parameters from a probability distribution used for Bayesian inference statistical analysis and is widely used in Exoplanet characterization to derive orbital parameter posterior distribution and their uncertainty estimates.

Mean anomaly is an angle that describes the position of a planet as a function of time, assuming the planet is moving in a circular orbit with a constant angular speed and the same period as the planet in an eccentric orbit. The mean anomaly is used to calculate the instantaneous position of an exoplanet in its eccentric orbit.

SB1 & SB2 binary stars are spectroscopic binary star systems. In a single-lined spectroscopic binary (SB1), the primary star is much more luminous than the secondary, so only the spectral lines of the bright component are recorded. In contrast, a double-lined spectroscopic binary (SB2) has visible spectral lines from both stars, enabling the determination of the RVs of both components.

Spectroscopic orbital elements in the context of RV-derived Keplerian orbits the set of derivable exoplanet parameters includes the orbital period P, the eccentricity e, the argument of periastron ω, the semi-amplitude K, and the time of periastron passage t_p, which together describe the shape and orientation of the exoplanet's orbit along the line of sight as well the planet's minimum mass if the stellar mass is known.

Thorium-Argon lamp is the most commonly used example of a hollow-cathode lamp, a standard calibration source lamp used in spectroscopy. It emits a well-understood spectrum of Thorium and Argon emission lines, providing accurate wavelength reference for precise RV measurements.

Time of periastron passage in the context of exoplanets refers to the specific moment t_p when an exoplanet is closest to its host star during its orbit.

True anomaly is an angle between a planet's position at periastron (the point in its orbit closest to the star) and its current position, measured from the focus of the orbit.

Nomenclature

AGN	Active Galactic nucleus
au	Astronomical Unit
BD	Brown Dwarf
CARMENES	Calar Alto high-Resolution search for M dwarfs with Exo-earths with Near-infrared and optical Échelle Spectrographs
ESPRESSO	Échelle SPectrograph for Rocky Exoplanets and Stable Spectroscopic Observations
ESO	European Southern Observatory
ELT	Extremely Large Telescope
F-P	Fabry-Pérot etalon
FOV	Field Of View
HARPS	High Accuracy Radial velocity Planet Searcher
HIRES	HIgh Resolution Échelle Spectrograph
HZ	Habitable zone
I_2	Iodine molecule
JWST	James Webb Space Telescope
LFC	Laser Frequency Comb
MCMC	Markov chain Monte Carlo
MS	Main Sequence
MMR	Mean Motion Resonance
NIR	Near-Infrared
PSF	Point Spread Function
RV	Radial Velocity
SNR	Signal-to-Noise Ratio
Th-Ar	Thorium Argon
UVES	Ultraviolet and Visual Échelle Spectrograph
VLT	Very Large Telescope

1 Introduction

The Doppler method has proven to be an indispensable technique for astronomers to precisely measure the kinematics of celestial objects such as stars, galaxies, and even the expanding Universe. The Doppler principle postulates that the frequency of waves changes depending on the relative motion between the wave source and the observer measured along the light of sight. In Astronomy, the Doppler method measures the wavelength shift of distinct spectral features in emission, absorption, or both caused by well-understood physical phenomena. In the context of stellar spectroscopy, we measure the dispersed electromagnetic intensity, where the Doppler effect is described in terms of the spectral absorption line shift in wavelength due to the motion of stars with respect to the observer. Neglecting the relativistic effects[1], the basic formula used to calculate the stellar spectral-line shift in wavelengths is:

$$\lambda' = \lambda \left(1 + \frac{v_r}{c}\right) \tag{1}$$

where, λ' is the measured wavelength, λ is the wavelength emits in the rest frame, v_r is the velocity of the star relative to the observer, and c is the speed of light. The shift of the stellar electromagnetic radiation spectra could be recorded and analyzed, and the line of sight (LOS) radial velocity component with respect to the observer is measured by simply:

$$v_r = c \left(\frac{\lambda' - \lambda}{\lambda}\right) \tag{2}$$

Figure 1 shows the structure of the optical spectrum of the Sun, which is a main sequence (MS) star of class G2 V. The Solar spectrum is not continuous across wavelengths and reveals distinct absorption lines caused by the presence of various chemical elements in the Solar atmosphere, such as light, and heavier iron-group elements like Carbon (C), Calcium (Ca), Chromium (Cr), Manganese (Mn), Magnesium (Mg), Cobalt (Co), Nickel (Ni), and Iron (Fe), among others. We know the exact wavelength positions of these spectral absorbers with extreme accuracy in the laboratory rest frame. Similarly, for other stars, we record their spectra and precisely measure the relative red- or blue-wavelength shift to determine the radial velocity (RV) of the object relative to the observatory. Thus, if a sub-stellar companion, such as an extrasolar planet (exoplanet), or Brown Dwarfs (BD) orbits a star, it induces the star to undergo a reflex motion around the system's center of mass (barycentre). The RV signal induced by an orbiting companion is very characteristic of and can be fully described by a

---

[1]Relativistic effects are important when studying objects moving at very high velocities near the speed of light, such as observation of high-redshift quasars, AGNs, and supernovae, which are key for testing the Hubble constant and the rate of the expanding Universe.
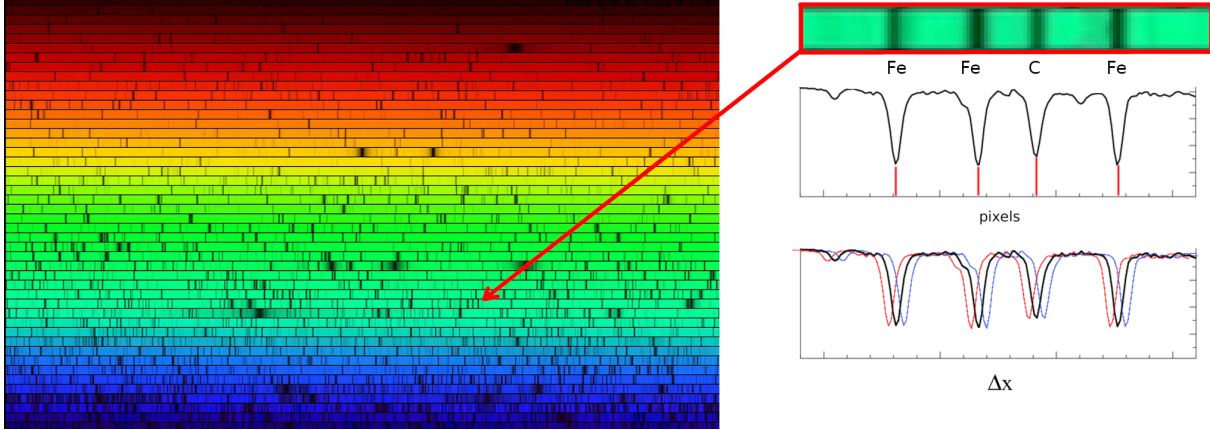
Fig. 1 Solar spectrum ranging from 392 nm (blue) to 692 nm (red), observed by the Fourier Transform Spectrograph at Kitt Peak National Observatory, Arizona, USA. The zoomed panel shows an example of absorption lines recorded on the CCD detector with well-known wavelengths. Measurements of red- and blue-Doppler shifts, crucial for detecting exoplanets, are achievable at the sub-pixel level.

Keplerian model. The RV signal amplitude and shape depend on the companion's mass and orbital geometry. For exoplanets, these Doppler shifts are rather small yet detectable by using modern spectrographs and have led to the indirect detection of over 1,100 exoplanets to date.

Important note

On "absolute" and "relative" Radial Velocity measurements
Each star has a unique direction of movement (e.g., in the Galaxy) relative to the observer analyzing stellar spectra. Consequently, each star will exhibit a Doppler shift, resulting in a consistent "absolute" radial velocity. In the context of detecting exoplanets, we are interested in measuring the differential, or hereafter, the "relative" radial velocities of stars with respect to their barycentre, rather than their absolute velocities. Absolute RVs are not important for orbit determination and are naturally subtracted during the Keplerian modeling.

Figure 2 shows a simple schematic of the Doppler method. To discover stellar or sub-stellar companions, such as a BD or an exoplanet, all we need to do is regularly obtain stellar spectra and measure their Doppler shift to determine the stellar radial velocities. From the characteristics of the RV signal as a function of time, a Keplerian model can reveal the spectroscopic parameters of the system, such as the orbital period and the orbital geometry of the perturbing object. Figure 2 also highlights the main disadvantage of the RV method. Wavelength shifts only allow us to measure the magnitude of the radial component of the stellar velocity (the red vector), which is along the LOS, while the tangential component of the velocity (the blue vector) remains unknown. With the Doppler method, we cannot determine the orbital inclination of the system, and therefore, we can only estimate the minimum mass of the perturbing companion (i.e., the exoplanet), not their true dynamical mass. Figure 2 illustrates that more massive but more inclined objects could, in principle, produce the same RV component vector. While the method itself seems fairly simple, as we will demonstrate further in this work, the precision RV measurements necessary to detect exoplanets are very complex and challenging.

1.1 History of the Stellar Doppler Technique in Astronomy

The first measurements of stellar radial velocity were done towards the end of the 19th century by the German astronomer Herman Carl Vogel, who used photography to record stellar spectra. Vogel's approach of recording spectra on photographic plates allowed researchers to systematically measure stellar RVs with a typical precision of a few $km\,s^{-1}$, which was sufficient to identify binary stars and stellar rotations. Systematic RV work has been performed at the Lick Observatory, which provides an extensive collection of Doppler measurements for bright stars, primarily observed between 1896 and 1926 using the Mills Spectrographs attached to the 36-inch refractor at Mount Hamilton (Campbell and Moore, 1926). Figure 3 shows such an example of archival RVs taken with photo plates from Lick and Victoria for the SB1 system HR 6388. The RVs could be measured only for the primary star, which is a K3 III giant star, thus far more luminous than the secondary companion. The photographic plate RVs have standard errors close to $1\,km\,s^{-1}$. In the 1970s Griffin (1978) complemented the HR 6388 observations by taking RVs using a photoelectric detector, slightly improving the RV precision, and leading to the firm binary orbit determination.

By the mid-20th century, astronomers managed to systematically record RVs of over 15,000 bright stars using photographic plates. Many of these targets were revealed as single (SB1) or double-line (SB2) binaries, and their orbital configurations were calculated based on the obtained RVs. Around that time, the visionary astronomer Otto Struve realized that precision was the only limit to detecting exoplanets. In the same way, binaries were uncovered, Struve postulated that RV measurements of a few hundred $m\,s^{-1}$ would be sufficient to detect close-in planetary companions with semi-major axes of about 0.02 au, and masses similar to that of Jupiter. Otto Struve predicted a class of

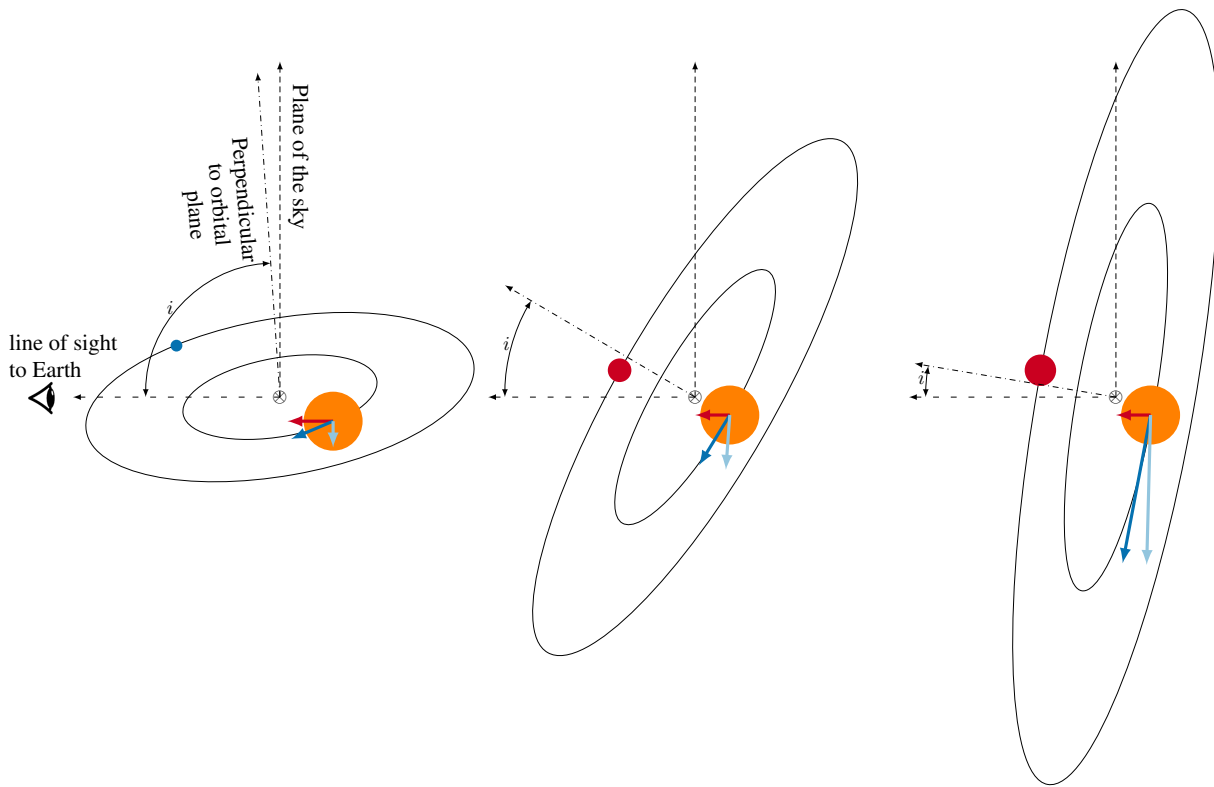**Three different stellar-substellar companion systems, each with a different line-of-sight inclination**

Fig. 2 The Doppler method measures the gravitational influence of an orbiting body (blue and red circle) on its host star (orange circle), detectable as a shift in the star's spectral lines due to the radial component of the star's motion towards or away from the observer. While the star follows a Keplerian orbit influenced by its companion, we can only measure the component of this motion that is along the line of sight–the red vector, representing the radial velocity. The tangential velocity (light blue vector) and the true space velocity (blue vector) components of the star's velocity does not affect the spectral line shifts and thus remains undetectable using the Doppler method. Since the inclination of the system is generally unknown without additional observations, the Doppler method provides only a minimum mass estimate of the orbiting body, expressed as $m_p \sin(i)$, where m_p is the mass of the companion, and i is the inclination of the orbit to the line of sight.

exoplanets now known as Hot-Jupiters (HJs) decades before the actual discovery of HJ exoplanets like 51 Peg b (Mayor and Queloz, 1995). Furthermore, Struve's proposal for precision RV work for detecting exoplanets formulated the possibility of detecting exoplanet "eclipses," now known as the transit detection technique for exoplanets. His visionary ideas marked significant foresight into methods that would only be realized much later.

Early efforts in stellar RV measurements faced challenges, particularly regarding precision. Techniques evolved over time, with notable contributions from researchers like Griffin (1967), who proposed strategies for improving Doppler precision by using photomultiplier detectors to scan the spectra along the direction of dispersion and calculate photoelectric RV measurements, reaching a steady precision of approximately $1 \, \text{km} \, \text{s}^{-1}$. Subsequent advancements, such as the development of gas cells (Campbell and Walker, 1979) and simultaneous calibration with Thorium-Argon (Th-Ar) lamps (Baranne et al., 1996), further refined RV measurement techniques, leading to unprecedented levels of precision by the early 1990s.

1.2 The Exoplanet revolution

Early Doppler surveys of exoplanets began with the observations by Campbell et al. (1988), who systematically monitored 16 stars for exoplanetary companions. They employed a hydrogen fluoride (HF) gas cell as a wavelength calibration source (Campbell and Walker, 1979), achieving an unprecedented precision at the time of approximately $\sim 13 \, \text{m} \, \text{s}^{-1}$. This precision was sufficient to detect Jovian-mass planets, but the limited sample size prevented definitive detections. Nonetheless, Campbell et al. (1988) noted that seven stars exhibited evidence of long-term, low-level variations. Among these, the K3 III giant star γ Cep A displayed RV variations, which could be potentially induced by a planetary companion. Subsequently, Walker et al. (1992) dismissed this interpretation, attributing the RV signal to the stellar activity of the red giant, influenced by theoretical prejudices against the existence of short-period giant planets. The existence of the
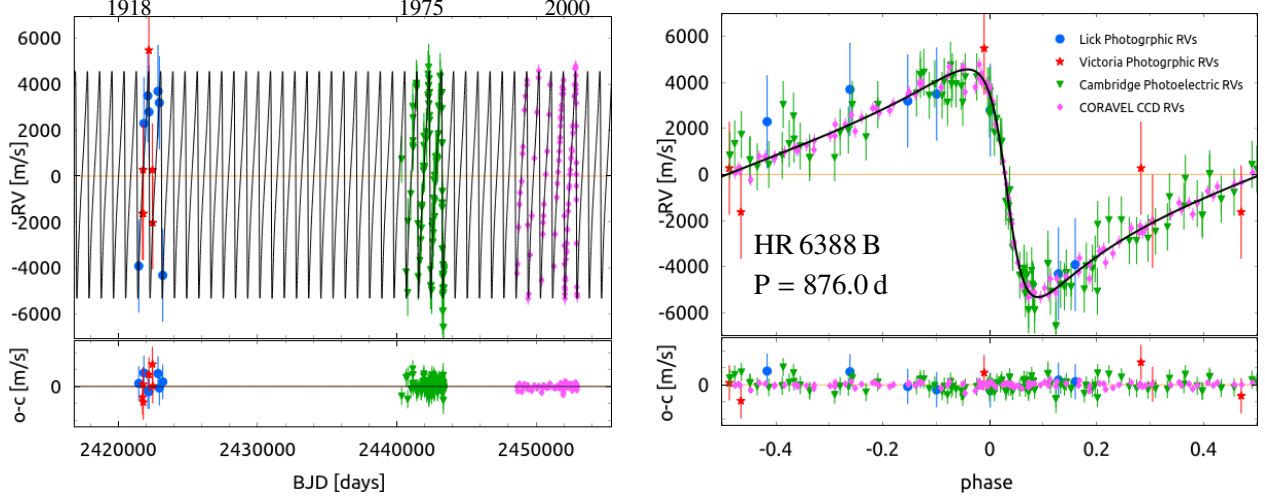
Fig. 3 RV measurements of the primary component of the SB1 binary HR 6388, of which first RV measurements were taken over 100 years ago (the top axis lists years). The left panel shows the RV time series, illustrating the long-term observational campaign. The earlier RVs were obtained from Lick Observatory using photographic plates (blue), from Victoria using photographic RVs (red stars), more recent measurements by Cambridge using photomultiplier technology in the 1970s, and finally newer CCD-based RV observations taken with the CORAVEL spectrograph. The right panel displays the phase-folded model and RVs, revealing the large binary signal. The small panels below the main panels show the residuals (observed minus calculated, or o−c) of the model, highlighting the differences between the observed RV data and the model predictions.

exoplanet γ Cep A b was only confirmed nearly two decades later by Hatzes et al. (2003), who verified that the RV variations of the primary binary component were indeed caused by a 1.7 M_{Jup} exoplanet with an orbital period of ∼2.5 yr.

In the late 1980s, (Latham et al., 1989) identified "A probable brown dwarf" orbiting the star HD 114762. With a period of approximately 84 days and a minimum mass of about M_{Jup}, this object exhibits characteristics of what we now call warm massive Jovian planets. Throughout the early 1990s, astronomers such as Hatzes and Cochran (1993) observed long-period RV variations in giant stars, suggesting the presence of giant planetary companions. These findings were later confirmed, notably for the star β Gem, solidifying the role of RV measurements in detecting exoplanets.

The discovery of a 'hot Jupiter' exoplanet around the solar-type star 51 Peg by Mayor and Queloz (1995) marked a revolutionary turning point[2] in the exoplanet search. Utilizing the ELODIE Échelle spectrograph (Baranne et al., 1996), mounted on the 1.93 m telescope at Observatoire de Haute Provence, pioneers Michel Mayor and Didier Queloz captured an unambiguous RV signal. This signal was consistent with a close-in giant planet orbiting its host star every 4.2 days. The minimum mass of the exoplanet was estimated to be 0.42 M_{Jup}, challenging existing models based on our Solar System and confirming the existence of the types of planets proposed by Struve four decades earlier. The left panel of Figure 4 displays the RV signal of 51 Peg, constructed from the original ELODIE RVs and supplemented by validation RVs obtained with the Hamilton spectrograph (Vogt, 1987) at Lick, USA by Marcy et al. (1997), along with high-cadence observations from the HARPS spectrograph (Mayor et al., 2003). The discovery of 51 Peg b significantly expanded the search parameters for exoplanets, shifting the focus to much shorter orbital distances and benefiting from improved precision in RV measurements.

Post-1995, the field of exoplanet research surged, with numerous astronomical groups adopting the Doppler method to hunt for exoplanets, which led to a rapid increase in exoplanet discoveries. Over the years, the precision of Doppler measurements has dramatically improved, with many RV instruments now capable of detecting velocity changes down to or even below 1 m s^{-1}. We can measure the velocity of stars many light-years away with precision comparable to a normal human walking speed! This high precision allowed astronomers to discover a planet in the habitable zone around our closest neighbor, Proxima Centauri (Anglada-Escudé et al., 2016).

The right panel of Figure 4 displays the RV signal of Proxima Cen b, detected using the UVES and HARPS spectrographs. Note the dramatic evolution in precision from the binary system HR 6388 to the first planet discovered around a Solar-type star, 51 Peg b, to our closest exoplanet neighbor, Proxima Cen b, as presented in Figures 3 and 4, respectively. The Stellar parameters and the best-fit models based on the RV data for these three systems are summarized in Table 1. Details on the model parameters and methodology can be found in Sect. 3. The significant increase in precision since the discovery of 51 Peg b has broadened the parameter space of detectable exoplanets, enhancing our understanding of their masses and orbits.

1.3 Impact of Doppler surveys for exoplanets

After the discovery of 51 Peg b, the next twenty exoplanets were discovered using the precise RV method. These discoveries were made using targeted RV surveys for exoplanets, which brought about many more planets in the coming years. In 1999, the first transiting exoplanet

---

[2]In 2019, Michel Mayor and Didier Queloz were awarded the Nobel Prize in Physics for this epochal discovery.
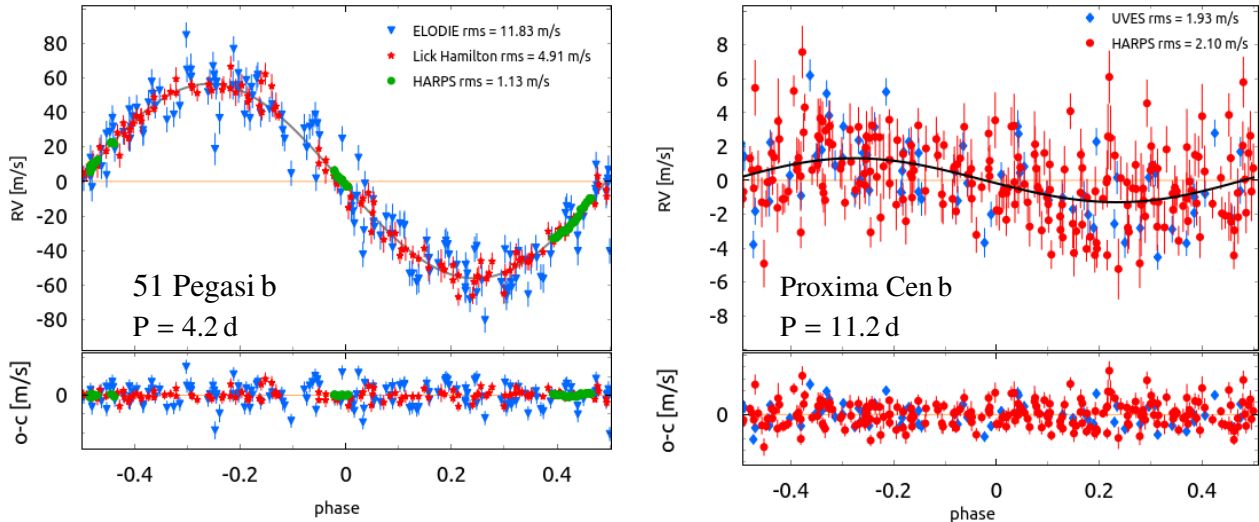
Fig. 4 The left panel shows the phase-folded RVs of 51 Peg, while the right panel shows the same for Proxima Cen, revealing the planetary-induced RV signal for these two stars. The top subplots list relevant information about the orbital period and the RV data used, along with their overall r.m.s. around the best fit. Same as in Fig.3, the bottom subplots display the RV model residuals.

discovered around the star HD 209458 by Charbonneau et al. (2000), marking a significant milestone in exoplanet research, providing a new method to study the exoplanet demographics. To date, the search for extrasolar planets has yielded over 5500 confirmed planets, with more than 900 systems with multiple planets[3]. Notably, the Doppler method of measuring stellar RVs has led to the discovery of over 1100 exoplanets, while the transit photometry technique, predominantly driven by the highly successful *Kepler* space telescope (Borucki et al., 2010), and recently the *Transiting Exoplanet Survey Satellite* (*TESS*; Ricker et al., 2015) has unveiled at least 4500 confirmed planets (which are usually validated with additional RV measurements!). The remainder has been detected through direct imaging (e.g., Marois et al., 2008), gravitational microlensing (e.g., Gaudi, 2012), or other methods.

Important note

On transiting versus RV exoplanets
A transiting exoplanet is detected when it passes in front of its host star, causing a characteristic periodic dimming in the star's brightness, which reveals the exoplanet's radius. Transit detection is only possible for exoplanet orbits nearly aligned ($i \sim 90°$) with the observer's line of sight. Many transiting exoplanets have been discovered because the method allows for the simultaneous observation of many targets with high photometric precision at a relatively low cost. In contrast, the RV method can detect Doppler shifts from both transiting and non-transiting planets but is operationally expensive and limited to a few hundred bright stars per survey. The transit method reveals the orbital inclination i but is not sensitive to the companion's mass, which can lead to false-positive detections of stellar companions. Therefore, knowing i, RV measurements are essential to validate the planetary nature of transit events by measuring the companion's mass.

Figure 5 presents a histogram of the exoplanet detection history by year (left) and cumulative (right), highlighting the progression and impact of detection techniques over time. Currently, astronomers have several techniques to detect and characterize exoplanets, but the two most efficient are the Doppler and the transit photometry techniques. The RV method has had a steady detection rate over the years due to long-lasting, precise RV surveys. After 2010, the ground-based transit monitoring for exoplanets also revealed exoplanets at an increased rate, surpassing the RV detections. A few notable sharp peaks in the histogram are associated with the bulk of exoplanets announced by the *Kepler* and *TESS* space telescopes.

The left panel of Figure 6 illustrates the exoplanet demography by showing the distribution of exoplanet mass versus orbital distance as revealed by the Doppler and transit detection techniques. The distribution of exoplanets is significantly influenced by observational biases inherent to these methods. Both techniques are exceptionally prompt at detecting more massive and shorter-period planets due to their higher detectability – the larger and more massive the exoplanet, the greater the induced RV and transit signals. Improved precision over the past two decades has also enabled the detection of a plethora of short-period, low-mass exoplanets, ranging from rocky bodies slightly larger than Earth to mini-Neptunes, thus introducing a new class of exoplanetary bodies, which to a large degree came as a surprise to astronomers. The Doppler method is sensitive to long-period colder massive companions similar to Jupiter, thanks to the long observational baselines of RV surveys. We have discovered a large number of these exoplanets, typically more massive, but continuing the legacy RV surveys, we are on a quest to recover the occurrence rate of Saturn analogs in the near future. Both techniques still need a longer observational baseline and better precision for exoplanet analogs of Uranus, Neptune, and the inner solar system planets.

---

[3] up-to-date list is available on https://expolanet.eu

Table 1 Best fit orbital parameters, minim masses, and semi-major axis alongside their 1σ uncertainties for the RV model fit presented in Figures 3 & 4. These are for systems studied in this work; HR 6388, 51 Peg b, and Proxima Cen b, using archival and literature RVs and modeled with the Exo-Striker tool.

Primary	HR 6388 A	51 Peg	Proxima Cen[a]
Sp. type	K3 III	G2 IV	M5.5 V
Mass ($M_\odot$)	1.02	1.11	0.12
Radius ($R_\odot$)	18.8	1.27	0.14
[Fe/H] (dex)	-0.17	0.2	-0.04
$T_{\text{eff.}}$ (K)	4335	5793	3306
distance (pc)	82.04	15.53	1.302
Companion parameters	HR 6388 B	51 Peg b	Proxima Cen b
P (d)	$876.3^{+0.1}_{-0.1}$	$4.2308^{+0.0001}_{-0.0001}$	$11.184^{+0.001}_{-0.001}$
K (m s^{-1})	$4915.8^{+40.0}_{-39.7}$	$56.4^{+0.4}_{-0.4}$	$1.25^{+0.16}_{-0.16}$
e	$0.621^{+0.005}_{-0.005}$	$0.008^{+0.006}_{-0.005}$	$0.035^{0.03}_{-0.02}$
ω (deg)	$97.2^{+0.9}_{-0.9}$	$304.4^{+29.4}_{-16.0}$	$259.0^{+64.3}_{-89.7}$
Ma (deg)	$45.2^{+1.3}_{-1.2}$	$324.7^{+15.9}_{-29.5}$	$207.0^{+89.7}_{-64.6}$
Mass (m sin i)	$0.197^{+0.002}_{-0.002}$ ($M_\odot$)	$0.480^{+0.003}_{-0.003}$ (M_{Jup})	$1.06^{+0.13}_{-0.13}$ ($M_\oplus$)
a (au)	$1.914^{+0.001}_{-0.001}$	$0.0530^{+0.0001}_{-0.0001}$	$0.04828^{+0.0001}_{-0.0001}$
Epoch	2421463.710	2449610.527	2451634.731

a - Note that at least one more confirmed exoplanet in the Proxima Cen system on shorter orbit (Faria et al., 2022), and an additional long-period candidate exoplanet (Damasso et al., 2020) which signals were not modeled in this work.

One of the ultimate goals in the exoplanet field is to determine the occurrence rate of Solar System analogs, particularly Earth-like planets capable of sustaining life. Achieving this goal requires an observational baseline on the order of decades with extremely precise RV measurements on the order of a few cm s^{-1}, which unfortunately remains beyond our reach to date. Consequently, we must rely on existing observational data to refine and calibrate our theories of planet formation, striving for a deeper understanding of these mechanisms and indirectly uncovering the observational diversity.

RV surveys have greatly enhanced our knowledge of exoplanet diversity and their potential formation processes. For instance, despite the high detection rate of HJs, we know that these objects are relatively rare, with only about 1% of Solar-type stars hosting HJs, and an even lower fraction among lower-mass stars (Sabotta et al., 2021). Many RV-detected planets are found in multi-planet systems, providing valuable insights into their dynamical interactions, which trace their formation history and evolutionary paths. The existence of HJs and multiple-planet systems close to or locked in mean-motion resonance (MMR) has opened a new field in astrophysics, aiming to explain their formation and advancing the theories of convergent giant-planet migration (e.g., Lee and Peale, 2002).

The right panel of Figure 6 depicts the distribution of exoplanet eccentricity versus orbital period. Measuring the eccentricity of hundreds of exoplanets with RVs has been a crucial factor in understanding the planet's formation and evolution pathways. The RV method, alone or in combination with transit observations, has revealed that many exoplanets possess moderate to highly elliptical orbits, contrasting with the nearly circular orbits observed in our Solar System. This observation is attributed to planet-planet scattering events during exoplanet evolution, suggesting some violent history of exoplanets (Ford and Rasio, 2008). Another critical output of evidence is that we owe the dedicated Doppler surveys the detailed planet occurrence rates as a function of the stellar host mass and metallicity (e.g., Fischer and Valenti, 2005; Wolthoff et al., 2022), which suggests a positive correlation between stellar metallicity and the occurrence rate of planets. By providing detailed insights into planets' mass, orbit, eccentricity, and period, Doppler surveys have enriched our comprehension of the dynamic architectures of planetary systems, highlighting their diversity and complexity.

2 Measuring precise Radial Velocities

Doppler surveys utilize high-resolution spectroscopy to measure the small periodic wobbles in the motion of stars, which result from the gravitational pull of orbiting planets. The development of sensitive spectrographs, coupled with the stable wavelength calibration of spectra recorded on Charge-Coupled Devices (CCDs), and precise RV extraction numerical routines are critical for the precision of RV measurements. In this section, we introduce the fundamental principles required to measure precise RVs.
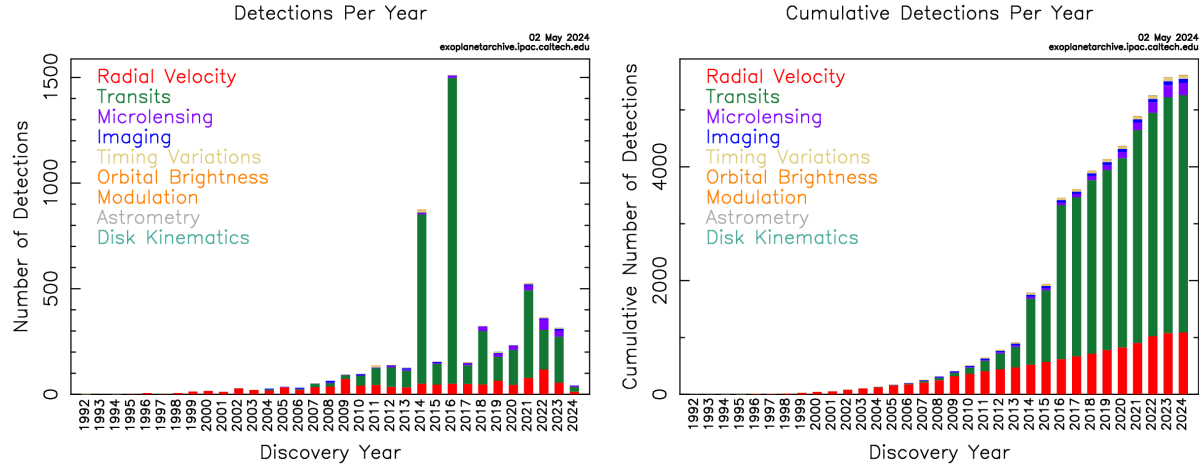
Fig. 5 History of exoplanet detection. The left plot shows the number of exoplanet discoveries per year. The right plot shows cumulative discoveries in each year, divided into the different detection methods. Image credit: NASA Exoplanet Archive; Courtesy NASA/JPL-Caltech.
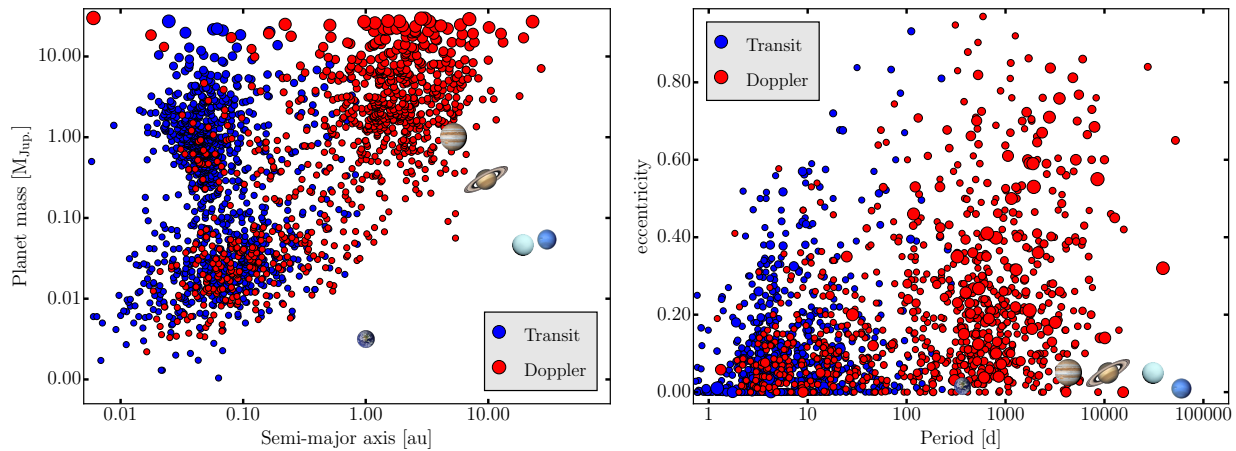

Fig. 6 Exoplanet demography revealed by the two most successful detection techniques: the Transit photometry (blue) and the Doppler RV (red) techniques. Larger symbols notate larger planetary mass. The left panel highlights detection biases favoring more massive and warmer planets, making solar system analogs and exo-Earths beyond reach at present days. The right panel, shows the period-eccentricity distribution, revealing a prevalence of exoplanets with moderate to high eccentricities, contrasting with the Solar system. Data are collected from the "Encyclopaedia of exoplanetary systems" (https://exoplanet.eu).

2.1 Modern Échelle spectrographs

Detecting the bulk of exoplanets through precision RVs has only become feasible thanks to the significant technological advancements over the past half-century. A major turning point in precision RV work was the introduction of CCDs as alternatives to photo plates and photomultiplier detectors. The highly efficient CCDs enabled the digital recording of high signal-to-noise ratio (SNR) spectra, allowing for the calibration and analysis of data using numerical techniques. However, classical long-slit spectrographs were not ideally suited for precision RV exoplanet hunting due to their limited wavelength coverage and relatively modest spectral resolution.

To effectively use stellar photons, astronomers and optical engineers needed to expand the wavelength coverage and resolution to record more spectral lines simultaneously on the CCD. This led to the brilliant concept of Échelle[4] spectrographs, which provide high resolving power R over a very large wavelength range. The resolving power R is defined as:

$$R = \frac{\lambda}{\Delta\lambda} \tag{3}$$

where λ is the wavelength of light, and $\Delta\lambda$ is the smallest difference in wavelength that the instrument can resolve. This defines the

---

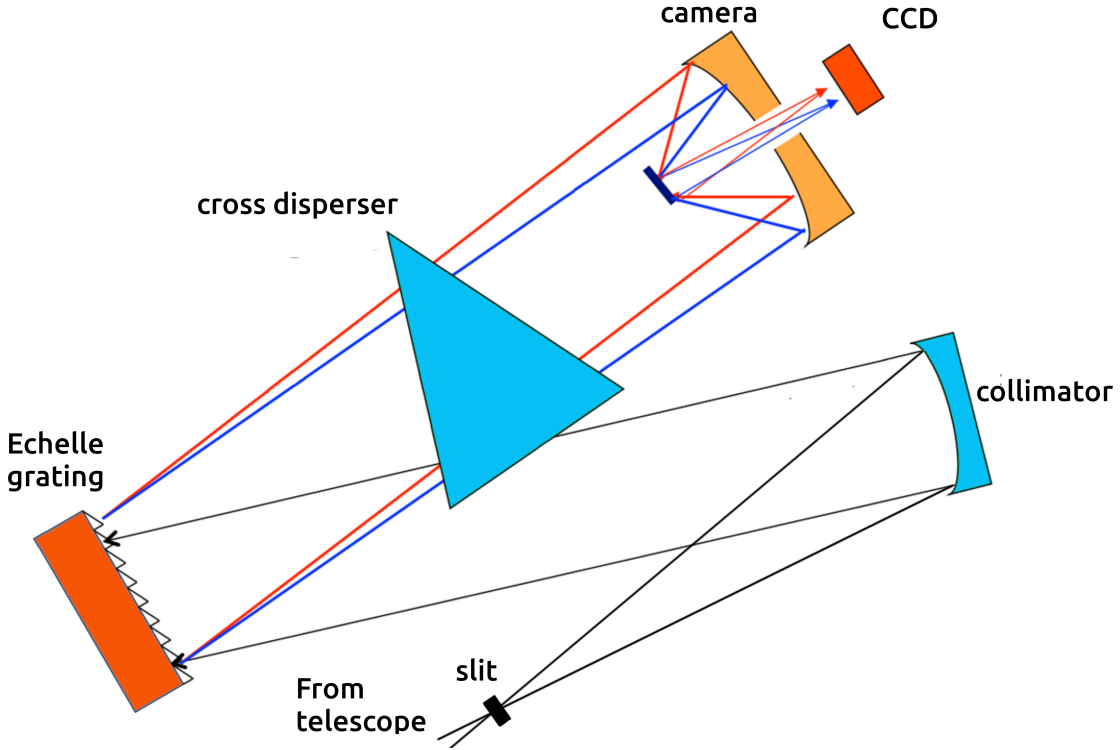[4]Échelle comes from the French word for "ladder."

Fig. 7 A simplified diagram of an Échelle spectrograph. In addition to the grating dispersive element, there is a second cross-disperser optical element, which is usually a prism.

instrument's ability to distinguish between two closely spaced spectral lines. Échelle spectrographs typically have $R \equiv \lambda/\Delta\lambda \sim 40\,000 - 120\,000$ and provide wavelength coverage in the region 380-900 nm (which varies widely across different designs), where CCDs are most efficient.

Figure 7 shows a simplified schematic of a modern Échelle spectrograph. Note that many design variants exist depending on the telescope's optical systems and the goals of the scientific programs. It is important for the reader to recognize that the Échelle spectrographs are considerably more complex than what is illustrated in Fig. 7. More details on Échelle spectrograph concepts can be found in the dedicated book of Eversberg and Vollmann (2015).

Briefly, an Échelle spectrograph has an entrance through which light from the telescope passes. Modern Échelle spectrographs are usually fed with an optical fiber, which sends the light from the telescope focus to the spectrograph. As we will discuss later, the spectrograph is usually placed in a separate temperature-stabilized room to ensure stability. Thus, the usage of a well-selected optical fiber is critical for the performance of the instrument. Telescope light from the fiber enters the spectrograph via an image slicer, which is an optical element that divides a light beam into narrower beams to increase the resolution and efficiency of a spectrograph, and thus is one of the components defining the resolution of the instrument. A collimator mirror with the same focal ratio as the telescope makes the light beam parallel to the first dispersing element; an Échelle diffraction grating. Échelle gratings have a relatively small grating constant and a large angle of incidence, resulting in many overlapping wavelength intervals in high orders (Eversberg and Vollmann, 2015). These overlapping orders are hardly useful. However, this "defect" could be converted to a useful "effect" by employing a second cross-disperser prism, which disperses the orders along the y-axis. Finally, the cross-dispersed orders are focused by a camera, which projects the spectra onto the CCD, filling most of the detector with useful spectra across many orders. This is illustrated in the left panel of figure 8, which shows a real spectrum (artificially colored, however) from the Optical arm spectrograph of the CARMENES instrument (see, Reiners et al., 2018, and reference therein). The right panel of figure 8, shows the extracted orders into one-dimensional spectra, ready to be wavelength calibrated and the RVs extracted.

To summarize, Échelle spectrographs offer:

- **High spectral resolution** – Échelle spectrographs can separate spectral features that are very close in wavelength, which is particularly important for precision RV work.
- **Large Wavelength Coverage** – The broad wavelength range of Échelle spectrographs makes them highly efficient for capturing a wide array of astronomical phenomena in a single exposure. In the context of exoplanet studies, the extensive wavelength coverage provides a sufficient number of stellar lines to measure precise RVs. Additionally, it helps differentiate between signals caused by stellar activity and those caused by companions. Doppler shifts due to companions are wavelength-independent, whereas activity-induced shifts are
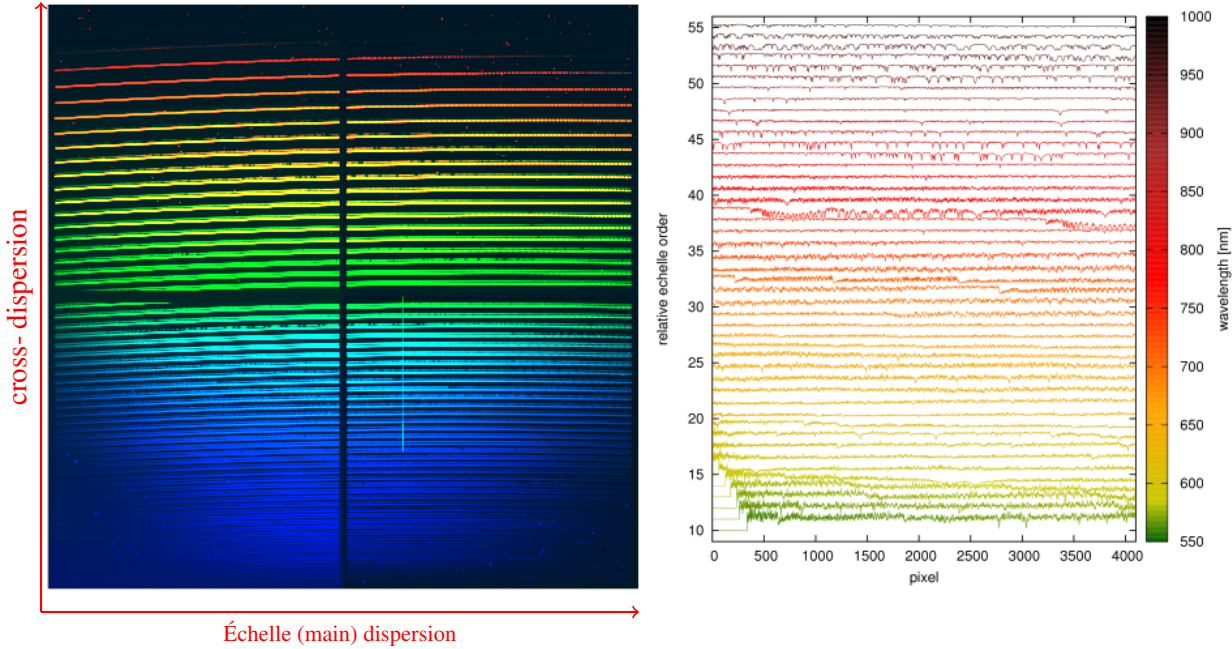
Fig. 8 The left panel displays the resulted échelle spectra on a CCD detector. The right panel shows the order-by-order wavelength calibrated 1D extracted spectra from which RVs are extracted. The spectra were taken for Luyten's star (GJ 273) with the CARMENES spectrograph and provided by Adrian Kaminski and Mathias Zechmeister (priv. communication).

not.

- **Compact design** – generally, Échelle spectrographs are compact instruments for 3-m class telescopes, although this depends on many factors. Some Échelle spectrographs on 8-m class telescopes such as ESPRESSO take considerable area in the VLT's Combined Coudé Laboratory. Only the vacuum tank alone is approximately 2 meters in diameter and about 4 meters in length, making it a large and sophisticated, *state-of-the-art* piece of equipment.
- **Versatility** – given the above, these instruments can be used for a wide range of spectroscopic interests, depending on specific observational needs, as long as the task is feasible. For instance, HIRES at Keck Observatory in the USA is a general-purpose spectrograph that has led to the discovery of over a hundred exoplanets.

Despite these advantages, Échelle spectrographs are complex and costly to construct and operate. Their data processing is also very challenging, requiring sophisticated techniques to separate and calibrate the overlapping spectral orders. Additionally, these complex instruments must maintain very stable temperature and mechanical conditions to achieve $m\,s^{-1}$ RV precision, as we will discuss in the following sections.

2.2 Wavelength calibration

Figure 8 illustrates that modern Échelle spectrographs record spectral intensity on a CCD detector. However, measuring Doppler shifts directly in the CCD pixel space is impossible. Each time we point the telescope at our stellar target to record its spectra, the absorption lines fall at different pixel positions. Moreover, stellar line shifts consistent with exoplanet signals occur at a sub-pixel level, but depending on the resolution of the spectrograph and the pixel size of the CCD, a typical shift of a single pixel can be transferred to a change in RV between 1 and 3 $km\,s^{-1}$. So, how are we expected to measure the Doppler shift down to $m\,s^{-1}$ precision? To achieve this, it is necessary to convert the relatively sparse pixel space to a finer grid of wavelengths. This is a standard technique achieved by calibrating our spectrograph with a stable calibration source. For exoplanet studies, the calibrator must remain consistent over many years to precisely measure the relative Doppler shift as a function of time. It is important to recall that achieving the desired RV precision ultimately relies on statistics by measuring the Doppler shift of as many stellar lines as possible in the calibrated wavelength space. Here, we discuss the two most common techniques for wavelength calibration, which are essential for detecting exoplanet signals.

2.2.1 The I_2 cell method

The I_2 cell method provides an efficient and inexpensive way to achieve long-term precision RV measurements in general purpose Échelle spectrographs. The application to stellar RV work was proposed by Marcy and Butler (1992), who demonstrated that placing an I_2 gas cell in the light path at the entrance of the spectrograph, provides many narrow and very well-defined I_2 spectral lines, which can be used as a wavelength reference.

Figure 9 shows a simplified scheme of the I_2 cell method. I_2 gas cells are favored for their rich spectrum of narrow absorption lines
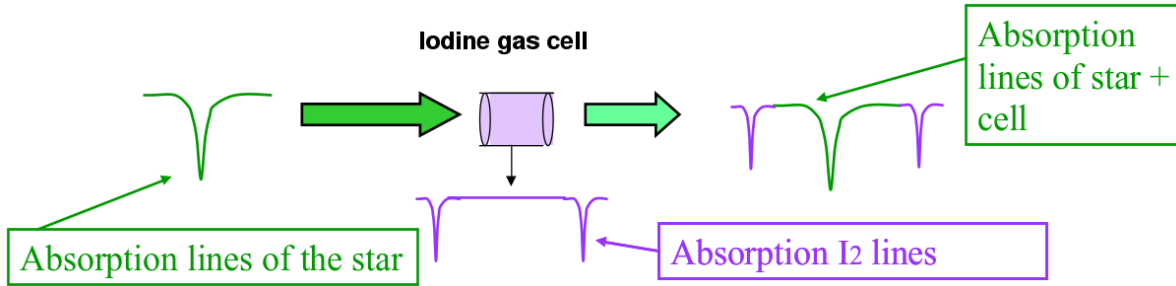
Fig. 9 The iodine cell method scheme. Light from the telescope passes through a glass chamber filled with I_2 gas. The absorption spectrum of the I_2 is superimposed onto the stellar spectrum, serving as a very stable wavelength reference. Credit: Figures are from Artie Hatzes's lecture notes (priv. communication), modified by the author.
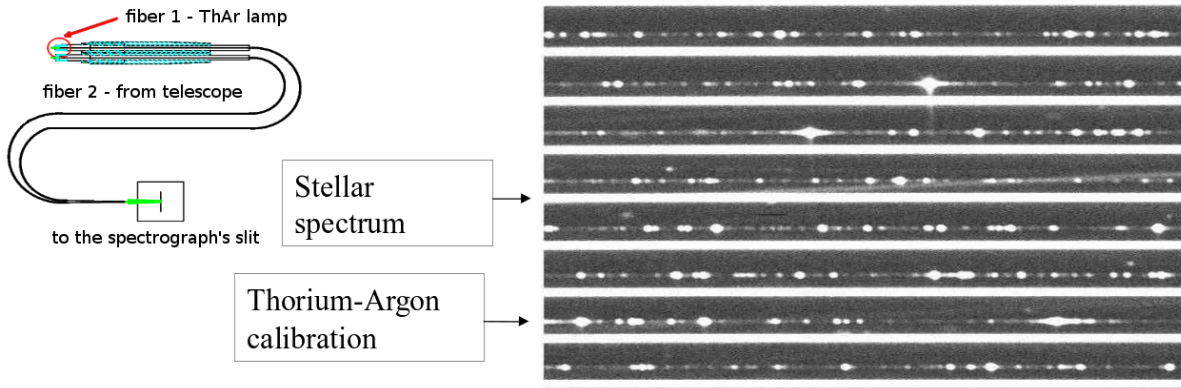

Fig. 10 A spectrum recorded with the HARPS spectrograph using a simultaneous Th-Ar calibrator lamp. Two optical fibers are illuminated simultaneously: one from the telescope and the other from the Th-Ar lamp. The seemingly continuous spectral orders are stellar spectra from the star fiber, whereas the Th-Ar spectrum consists of strong emission lines used for wavelength calibration. Credit: Figures are from Artie Hatzes's lecture notes (priv. communication), modified by the author.

within the 500-600 nm wavelength range, providing very stable reference lines superimposed on the stellar spectra. The I_2 cells offer practical benefits such as compact size, ease of use, and low maintenance. These devices do not require additional optics, making them an ideal upgrade for high-resolution general-purpose spectrographs whose primary goal was not initially exoplanet surveys. This means that any suitable spectrograph could be transformed into a precision RV machine. The main requirement is to maintain a constant operating temperature near 50°C. The HIRES spectrograph was the first Doppler instrument capable of delivering precise RVs down to 3 m s^{-1}, or even better for dwarf stars (Butler et al., 1996). Through ongoing instrument and RV extraction pipeline optimizations, precision has significantly improved over the years, reaching about 1 m s^{-1} for bright stars (Butler et al., 2017). Over the years, many other Échelle spectrographs were equipped with an I_2 gas cell for detecting exoplanets, proving to be very effective.

There are, of course, some operational challenges with the I_2 method. For instance, the data reduction and RV extraction processes are complicated. First, obtaining very high-resolution spectra of the I_2 gas cell and constructing a model template is required. Although this is needed only once, only a few facilities worldwide can scan spectra with a resolution (R > 500,000), which is necessary for this task. Additionally, high SNR spectra without the I_2 spectra for each studied star must be obtained, known as a "stellar template", which consumes traditional operational time. The I_2 lines contaminate the stellar spectrum, complicating or even preventing further spectral analyses such as abundance studies or examining spectral line shapes needed for stellar activity analysis.

Despite these challenges, the I_2 method remains an excellent tool for studying the occurrence rate of Jovian analogs. This task does not require extreme cm s^{-1} precision but does need a long-term baseline of stable RV reference, which is easily achieved with I_2 cells. Legacy and future RV surveys using spectrographs equipped with I_2 cells are relatively inexpensive to build and maintain, potentially revealing many more massive exoplanets in the coming decades.

2.2.2 The simultaneous Th-Ar calibration method

The Thorium-Argon (Th-Ar) lamps have been widely used as a wavelength calibration source in astronomy for many decades due to their advantages in spectral analysis. Thorium, serving as an excellent cathode, offers a dense array of narrow spectral lines across visible wavelengths, which helps in accurate wavelength calibration. A key technique involves recording the Th-Ar spectrum simultaneously with the stellar spectrum using optical fibers. This setup involves using one fiber optic to channel light from the star and another for light from a calibration lamp to the spectrograph, where both spectra are recorded side by side on the CCD detector. This method ensures that any
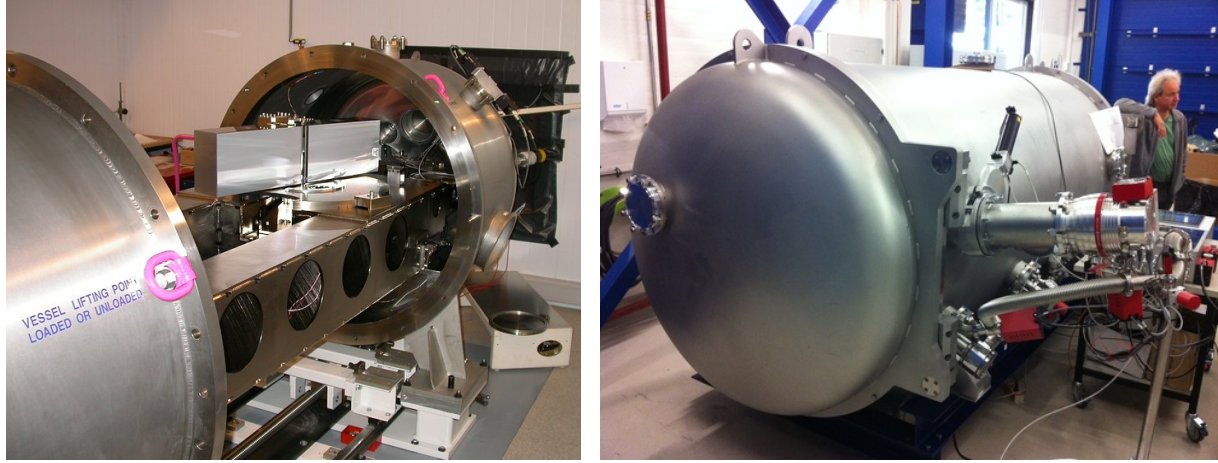
Fig. 11 The left panel shows the optical bench of the HARPS spectrograph, which resides inside a vacuum tank (opened in the picture) to maintain thermal stability. Credit: ESO. The right panel shows the vacuum tank of the CARMENES optical channel, with the CARMENES system engineer Walter Seifert for scale. Credit: CARMENES Consortium.

instrumental shifts affect both spectra equally, minimizing systematic errors in the wavelength calibration.

Figure 10 shows a simplified schematic of the method. A stellar spectrum from the telescope illuminates an optical fiber, whereas a second optical fiber is fed with Th-Ar lamp. Therefore, both Th-Ar and Stellar spectra are recorded simultaneously, and we can associate the CCD pixel coordinates with wavelengths given the well-known Th-Ar spectra.

The advantages of using Th-Ar lamps include their well-understood spectrum, thanks to decades of usage in the astronomical community. Th-Ar lamps offer broad wavelength coverage in the optical region from 300-700 nm, making them ideal for CCD detectors. Th-Ar calibration does not lead to light loss of the stellar spectra, which is beneficial for other types of stellar analysis, such as studying spectral abundance or line shapes.

However, Th-Ar lamps also have some well-known disadvantages. Beyond 650 nm, the density of Th-Ar emission lines decreases rapidly, making these lamps less suitable for calibration in the near-infrared. Another issue is that Th-Ar lamps "age", causing their emission spectra to change over time and "lose" lines, which poses a problem for consistent wavelength calibration over decades. Some Th-Ar lines are so bright that they lead to saturated lines, which "spill" over several spectral orders and add significant line contamination. Finally, aside from astronomy, Th-Ar lamps are not widely used, leading manufacturers to discontinue their production, making such lamps currently scarce.

2.2.3 Fabry–Pérot etalons and Laser Frequency Combs

Traditional calibrators like Th-Ar lamps and iodine cells provide long-term stability and high precision in RV measurements. However, achieving a Doppler precision of 1–10 cm,s^{-1} requires an additional layer of complex optomechanical engineering. In recent years, two advanced calibrators have been employed in combination with standard wavelength calibrators: Fabry–Pérot (F-P) etalons and Laser Frequency Combs (LFCs). The nature and implementation of the F-P and LFC are complex and will not be discussed in detail in this work. For a brief, yet very comprehensive explanation of these methods, we encourage the reader to refer to Hatzes (2019).

F-P etalons produce a dense spacing of transmission peaks that can be used for wavelength calibration. When actively controlled using atomic references, they can achieve Doppler precisions of a few cm s^{-1}. Despite their benefits, F-P etalons pose challenges due to the need for precise calibration of their optomechanical components. Their use, in combination with other calibration methods such as Th-Ar calibrators, can effectively correct instrumental drifts and improve wavelength calibration, thereby enhancing the overall precision of RV measurements.

LFCs provide a dense array of laser peaks, equally spaced in frequency over a broad bandwidth. This makes them superior to traditional calibrators like Th-Ar lamps and iodine cells, as they offer long-term stability, high precision, and known absolute wavelengths (when used together with ThAr lamps). LFCs have shown the potential to achieve RV precisions of about 1 cm s^{-1}, which is critical for detecting small exoplanets. However, LFCs are extremely complex and costly devices, and their usage is still in the experimental phase.

2.3 Mechanical and thermal stability

Thermal and mechanical stability are essential for long-term, precise RV measurements. To detect small, rocky exoplanets, the current gold standard employs simultaneous Th-Ar calibrated, ultra-stable Échelle spectrographs such as HARPS and CARMENES. Figure 11 depicts the HARPS and CARMENES instruments during their commissioning phase. For instance, HARPS is housed within a specialized vacuum vessel chamber, located in a dedicated room at the 3.6-meter telescope in La Silla, Chile, where access is strictly prohibited. The long-term RV precision of instruments like HARPS is due to their design, which includes robust insulation against temperature and pressure fluctuations and mechanical shocks, maintaining stability for years. This minimizes the thermal effects that can affect the mechanical and
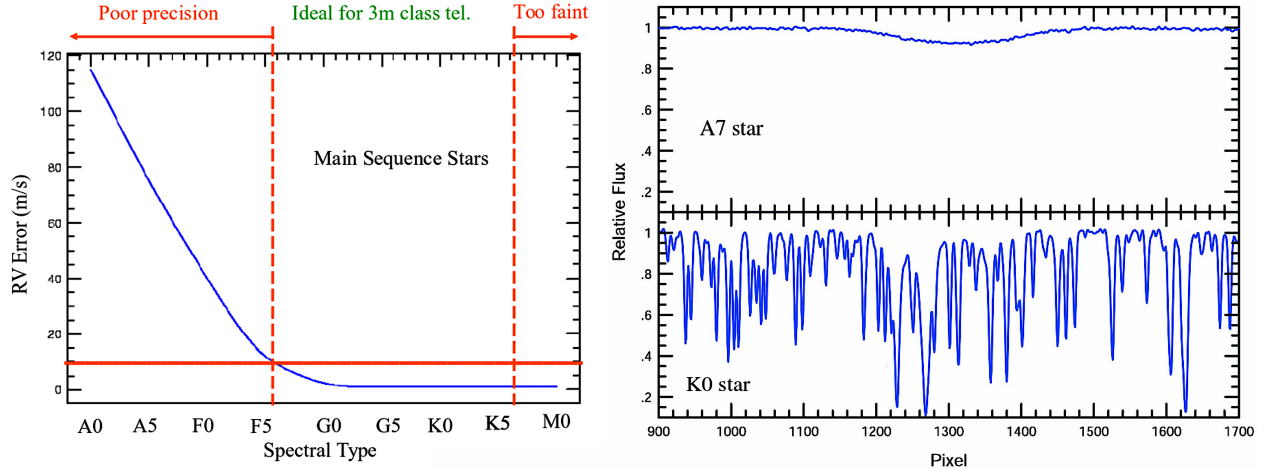
Fig. 12 The Left panel shows the typical RV precision as a function of stellar spectral type. The right panel shows the difference in spectra between a young massive star of spectral type A7 and a star of spectral type K0. The horizontal dashed line marks an RV precision of 10 m s^{-1}, necessary to detect a Jupiter-analog around a sun-like star. Credit: both figures are from Artie Hatzes (priv. communication).

optical components of the instrument, thus reducing noise and systematic errors in the wavelength calibration and the point-spread-function (PSF) instrument profile. Currently, the temperature stability of HARPS is maintained below 0.01 K (Lo Curto et al., 2024).

HARPS serves as a benchmark for ultra-precision RV instrumentation. No modern spectrograph designed to detect small rocky exoplanets is built or currently under construction without significant investments in thermal and mechanical stability. As technological advancements continue to extend the limits of achievable RV precision, addressing these instrumental and calibration challenges remains crucial for discovering Earth-like exoplanets in the habitable zones of stars.

2.4 RV Precision across Spectral Types

For a good reason, the RV exoplanet surveys mainly focus on stars with spectral types later than F5. The left panel of Fig. 12 shows the achievable RV precision as a function of stellar spectral type, while the right panel presents an example of recorded spectra for stars with spectral types A7 and K0. Stars earlier than F5 are typically younger, hotter, and rotate faster. As a result, they have fewer and more broadened stellar lines, making it difficult to measure RVs accurately. Therefore, young and hot stars are poor targets for precision RV work. Cooler stars of spectral type later than F5 have slower stellar rotation velocities. These stars are typically main-sequence (MS) and red giant post-MS stars of spectral types G and K. They possess many deep spectral lines, each containing Doppler information, which allows for the assembly of adequate RV statistics. Consequently, these stars are excellent targets for precision RV surveys. Moreover, most observed red giants of spectral types G and K are retired A-F intermediate-mass stars, for which reliable RV measurements cannot be obtained. Therefore, studying the exoplanet population around red giants provides valuable insights into the population around more massive stars than the Sun. From Figure 12, it is evident that these stars are ideal for precision RV measurements using relatively small telescopes, in the 2-3 meter class, and even smaller telescopes. Small telescopes are much cheaper to operate than larger 8-meter class telescopes, such as the VLT. Consequently, they are often used for RV surveys to take advantage of the lower operational costs while still achieving precise measurements.

As indicated in Figure 12 on the other side of the spectral classification, stars later than K5 were often too faint for practical observation with small telescopes. Late K and M red-giants are bright and suitable (e.g., Reffert et al., 2015), but these very evolved stars have been shown to show significant stellar activity, likely due to non-radial stellar pulsations. Late spectral type MS stars are the most abundant in the solar neighborhood. For instance, M dwarfs represent a large fraction – about 72% – of the stars within 10 pc (Golovin et al., 2023). While these stars are faint, they have presented significant interest to the scientific community. Exoplanets around K and M-dwarfs induce higher Doppler signals than in more massive stars such as the Sun because of the smaller mass ratio. The lower stellar masses allow for the detection of potentially rocky planets in the habitable zone (HZ), and multiple-planet systems with relatively packed shorter periods with typical RV semi-amplitudes of a few m s^{-1}.

For this reason, in recent years, it has become evident that acquiring precise RV measurements in the redder part of the spectrum significantly enhances M-dwarf surveys (Reiners et al., 2018). Among the instruments tailored for this purpose is the CARMENES spectrograph, which is specifically suited for measurements of M dwarfs. This is due to its operation in the red part of the visible and near-infrared (NIR) spectral regions, which reduces the influence of stellar activity on the RVs.

Consequently, most host stars of RV-detected planets fall within a mass range of 0.4−1.2 M$_\odot$, thus presenting a notable bias in the exoplanet demographics as a function of the stellar host's properties.

3 Modeling Radial Velocity curves

3.1 Extracting Keplerian orbits

To introduce the extraction of Keplerian orbitals from RV signals, we start with the simplest case of an exoplanet orbiting its parent star in a perfectly circular orbit with eccentricity $e = 0$. In this case, the argument of periastron ω becomes undefined because the concept of the point of closest approach to the star is not applicable. It is important to note that the Doppler method does not allow for the determination of the exoplanet's orbit in three dimensions, as the orbital inclination i and the angle giving the orientation of the orbit on the plane of the sky, called the longitude of the ascending node Ω, remain undefined. Therefore, for a companion on a perfectly circular orbit the parameters e, ω, i, and Ω do not contribute, and the stellar RV around the barycenter can be modeled by a cosine (or sine) model in the form:

$$V(t) = K \cos\left(\frac{2\pi}{P}(t - t_0)\right) + \gamma \tag{4}$$

where K is the semi-amplitude of the RV signal, P is the period of the exoplanet's orbit, t is the time, and t_0 is the reference epoch (often the time of periastron passage t_p when $e > 0$). Finally, γ in this context is the "absolute" radial velocity of the star with respect to the observer, which can be ignored at this point. In this case, $\frac{2\pi}{P}$ is the mean motion n of the planet, and together with the time after the reference epoch $t - t_0$, it defines the phase of the signal.

Including the eccentricity in the signal, modeling makes it more complex due to the non-sinusoidal, asymmetric, and non-linear nature of the RV curve. This leads to the so-called "RV equation," which for a single planet with an eccentric orbit has the following form:

$$V(t) = K\left[\cos\left(v(t) + \omega\right) + e\cos\omega\right] + \gamma \tag{5}$$

where ω is the argument of periastron of the star (since we measure the stellar RV movement, not the planet's), and we introduce another important time-dependent angle called the true anomaly $v(t)$, which is the angle normally used to characterize an observational orbit. To determine the function $v(t)$ over time, we must introduce two more important time-dependent angles known as orbital "anomalies": the eccentric anomaly $E(t)$ and the mean anomaly $M_a(t)$. The eccentric anomaly $E(t)$ is an angle used to describe the position of a planet in its elliptical orbit around a star, from which we can derive $v(t)$ using the following geometrical relation:

$$\cos E(t) = \frac{\cos v(t) + e}{1 + e\cos v(t)} \tag{6}$$

or, alternatively written, $v(t)$ can be derived from the $E(t)$:

$$\tan\left(\frac{v(t)}{2}\right) = \sqrt{\frac{1+e}{1-e}}\tan\left(\frac{E(t)}{2}\right) \tag{7}$$

We still have to solve $E(t)$, and for the purpose we need the mean anomaly $M_a(t)$ defined as:

$$M_a(t) = \frac{2\pi}{P}(t - t_p) = n(t - t_p) \tag{8}$$

which tells us how far an exoplanet has progressed with respect to the time of periastron passage t_p, or other arbitrary epoch. The eccentric anomaly $E(t)$ is related to the mean anomaly $M(t)$ through Kepler's Equation:

$$M_a(t) = E(t) - e\sin E(t) \tag{9}$$

which for a perfectly circular orbit with $e = 0$ it leads to Eq.4. Unfortunately, Kepler's equation cannot be solved analytically and needs some iterative approach. Fortunately, however, modern computational algorithms can solve this equation numerically with relative ease.

At this point, we are ready to model the RV shape of an exoplanet signal, and the only parameter that requires attention is the RV semi-amplitude K. In signal modeling, K is a fitting parameter independent of the physical reason for the observed semi-amplitude. Yet, we know that K provides information about the star-planet mass ratio, and if we know the mass of the star, from e.g., stellar isochrone models, which is often the case, we can get the minimum mass of the planet. The radial velocity semi-amplitude is expressed as:

$$K = \frac{2\pi}{P}\frac{a\sin i}{\sqrt{1 - e^2}}. \tag{10}$$

or alternatively one can get the projected semi-major axis of the star, measuring the RV signature of K, P, and e:
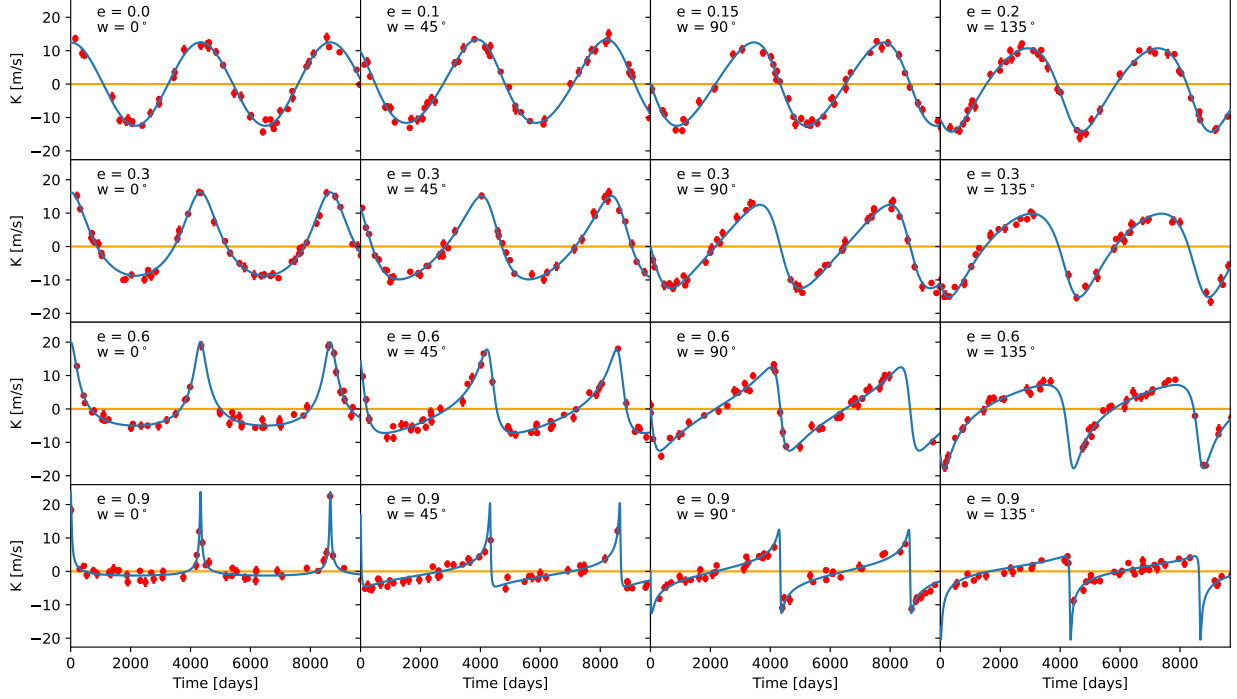
Fig. 13 RV signature of a single planet, consistent with the period and mass of Jupiter around a 1 $M_{\odot}$ star for different orbital geometries in terms of eccentricity e and argument of periastron ω. Red data are simulated RVs with the typical precision of HAPRS for solar-type stars.

$$a \sin i = \frac{KP\sqrt{1-e^2}}{2\pi}. \tag{11}$$

The value of the projected semi-major axis $a \sin i$, however, is a problem since a nor $\sin i$ can be determined separately. After making some transformations using Kepler's third law, the orbit of the star around the barycenter is given by the form:

$$P = \sqrt{\frac{4\pi^2}{GM}a^3} \tag{12}$$

where G is the gravitational constant and the total mass M, which to account for the unknown $\sin i$ leads to the mass function:

$$f(m) = \frac{m_p^3 \sin^3 i}{(M_{\star}+m_p)^2}. \tag{13}$$

and after some more transformations, we end up with the most common expression of the RV semi-amplitude:

$$K = \left(\frac{2\pi G}{P}\right)^{1/3} \frac{m_p \sin i}{(M_{\star}+m_p)^{2/3}} \frac{1}{\sqrt{1-e^2}}. \tag{14}$$

Estimates of $M_{\star}$ can be inferred from stellar models, which, rely on the observed photometric data, stellar luminosity, and effective temperature. From RV data fitting the spectroscopic observables K, P, and e could be used to estimate the minimum mass of the planet $m_p \sin i$, which is of our primary interest. Assuming the mass of the planet is $m_p \ll M_{\star}$, thus approximating to $m_p + M_{\star} \approx M_{\star}$, A common practical equation for K is often given as:

$$K = \frac{28.4329\text{m s}^{-1}}{\sqrt{1-e^2}} \left(\frac{P}{1\,\text{yr}}\right)^{-\frac{1}{3}} \left(\frac{m_p \sin i}{M_{\text{Jup}}}\right) \left(\frac{M_{\star}}{M_{\odot}}\right)^{-\frac{2}{3}} \tag{15}$$

Table 2 summarizes the period, eccentricity, semi-major axes, and calculated semi-amplitudes K of the planets in the Solar system. It is clear that if an alien civilization observes the Sun as a star and obtains stellar RVs with similar precision to what we currently have on Earth, the only planets likely to be detected are Jupiter and Saturn, with $K = 12.5$ m s^{-1} and 2.8 m s^{-1}, respectively.

Table 2 Orbital parameters and semi-amplitude of the planets in the Solar system.

Planet	P (years)	e	a (au)	K (m s^{-1})
Mercury	0.24	0.2056	0.39	0.008
Venus	0.62	0.0067	0.72	0.086
Earth	1.00	0.0167	1.00	0.089
Mars	1.88	0.0934	1.52	0.008
Jupiter	11.86	0.0489	5.20	12.48
Saturn	29.46	0.0565	9.55	2.76
Uranus	84.01	0.0463	19.22	0.30
Neptune	164.79	0.0097	30.11	0.28

Figure 13 shows the typical RV signature of simulated RVs induced by an exoplanet with 1 $M_{\mathrm{jup.}}$ at 5.2 au, orbiting a star with 1 $M_\odot$ (a Jupiter analog) for different orbital eccentricities and geometries in terms of ω. The simplest case is for $e = 0, \omega = 0$, shown in the top left panel, which is practically a simple sine model. By increasing e and varying ω, the signal becomes more complex.

Now we have a model with parameters $V(\theta)$, which are the five spectroscopic observables related to the star's Keplerian orbit: $\theta = \{e, P, M_a, \omega, K\}$ and the systemic RV velocity γ. If more than one planet is evident in the data, then a second set of these parameters should be included in the model, i.e., $\theta_n = \{e_n, P_n, M_{a,n}, \omega_n, K_n\}$, where n is the number of planets in the model. If more than one RV dataset is used, which is often the case (see Figs. 3 and 4), then we must also fit for the RV data offset γ_p for each dataset, where p is the number of datasets. Then we can find the maximum of the ln $\mathcal{L}$ function:

$$\ln \mathcal{L}(\theta) = -\frac{1}{2} \sum_{i=1}^{N} \left[\frac{(v_i - V(t_i; \theta))^2}{\sigma_i^2} + \ln\left(\sqrt{2\pi}\sigma_i \right) \right] \tag{16}$$

where v_i are the observed radial velocities, $V(t_i; \theta)$ are the model radial velocities at time t_i, and σ_i are the uncertainties in the observed radial velocities.

The ln $\mathcal{L}(\theta)$ function can be optimized using standard numerical techniques such as the Nelder-Mead simplex algorithm (Nelder and Mead, 1965), which converges to the best-fit solution, or through parameter sampling techniques such as Markov chain Monte Carlo (MCMC) sampling and the nested sampling methods, which are used for Bayesian inference analysis and posterior estimation of the sampled parameters consistent with the data.

3.2 Planet search using periodogram analysis

Detecting exoplanets using RV data cannot be done by eye, particularly for short-period planets with sufficient temporal baselines of observations. An additional challenge in the preliminary exoplanet vetting process is the complexity of RV data, which is profoundly affected by multiple RV signals (i.e., multiple-planet systems), significant RV noise (see Sec.4), uneven time sampling, and observational gaps due to Earth's rotation and seasonal changes. These factors can produce suspicious signals due to aliasing, making the RV data analysis ambiguous and complex.

Astronomers rely on automatic period search algorithms based on Fourier data analysis principles. Fourier's work demonstrated that any continuous function could be represented by a series of sines and cosines, simplifying the detection of periodic signals in time-series data. In the domain of RV data, this translates to identifying peaks in the Fourier transform that correspond to the frequencies of orbiting exoplanets. A popular tool for astronomers is the so-called "generalized" Lomb-Scargle periodogram (GLS Zechmeister and Kürster, 2009). The GLS is very efficient and fast at revealing dominant frequencies despite the data's irregular sampling and gaps, offering a robust way to analyze noisy datasets. In recent years, even more complex and accurate, yet CPU-intensive derivatives of the GLS have gained popularity. These include the maximum ln $\mathcal{L}$ periodogram (MLP), which is more robust for multi-telescope data, the Bayesian generalized Lomb-Scargle periodogram (BGLS), and others.

Periodograms provide the numerical stability and speed essential for managing the large volumes of data typically involved in exoplanet detection. Hence, periodograms remain a cornerstone technique for astronomers and astrophysicists engaged in the search for exoplanets through RV measurements, providing a critical tool for interpreting complex astronomical RV data.

3.3 Exoplanet characterization tools

Several exoplanet modeling programs are publicly available, with most developed in the modern Python3 language, designed to analyze exoplanetary orbits from data such as precise RVs and transit photometry. For instance, the Exo-Striker exoplanet toolbox could be of particular interest to the reader. This is an open-source program with a user-friendly Graphical User Interface (GUI), available for download at https://github.com/3fon3fonov/exostriker. Figure 14 shows a typical GUI view of the Exo-Striker exoplanet toolbox. Developed for both professional and educational use, Exo-Striker is suitable for postgraduate students and their tutors. It offers a comprehensive suite of features for the detailed analysis of both transit and RV data. This includes power spectrum analysis such as the GLS periodogram for identifying signals, Keplerian and dynamical modeling of multi-planet systems, and standard frequentist and Bayesian methods for orbital parameter estimation. The Exo-Striker also provides tools for long-term stability checks of multi-planet systems and generating
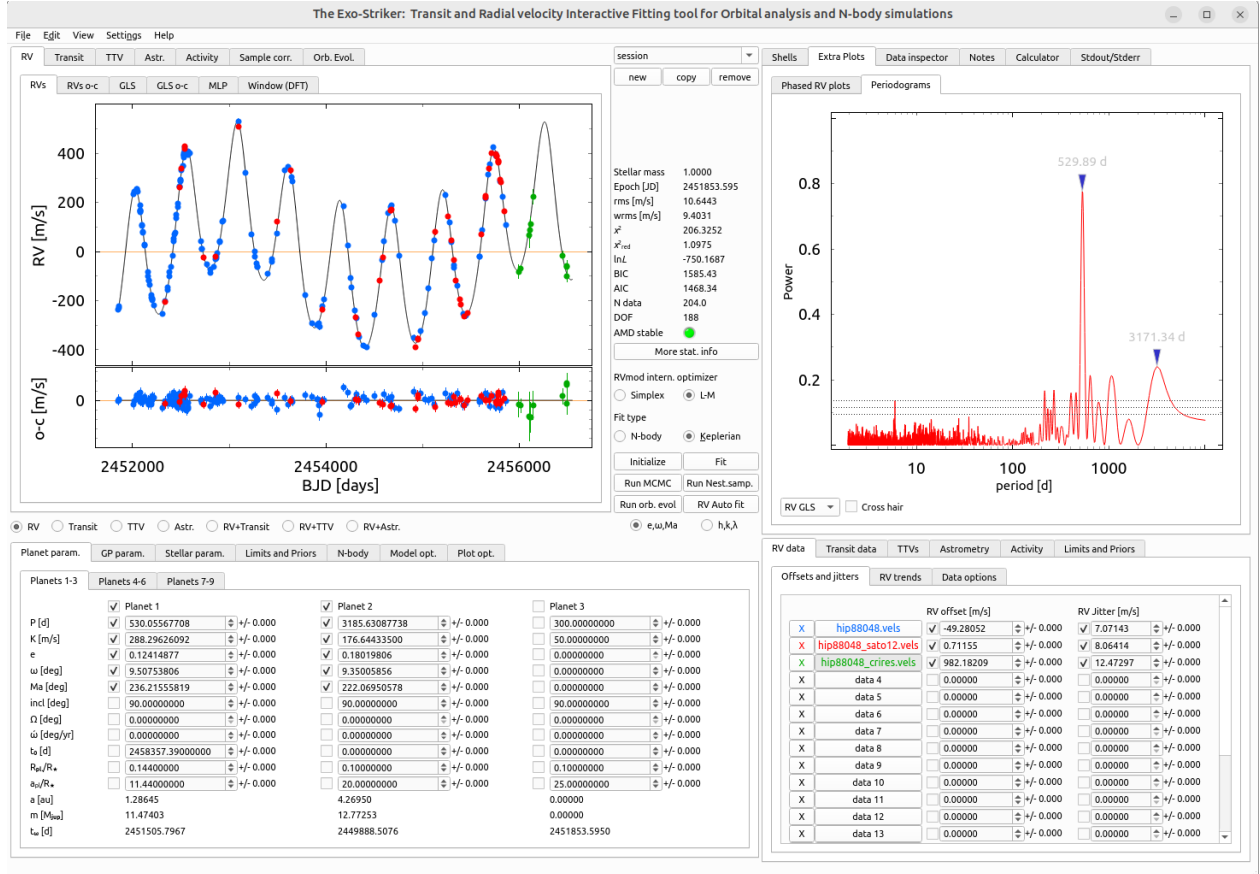
Fig. 14 GUI screenshot of the Exo-Striker tool analyzing the ν Oph multiple-planet system. The left panel shows a typical view of the GLS and RV fitting part, which provides fast plotting, parameter overview, and statistics.

fast interactive plots. Compatible with MacOS, Linux, and Windows, Exo-Striker is a versatile choice for astronomers and astrophysicists engaged in exoplanet discovery and characterization.

The orbital fits for HR 6388 B, 51 Peg b, and Proxima Cen b discussed in this work were conducted using the Exo-Striker, utilizing publicly available literature and archival RV data for these targets. The Exo-Striker sessions for these analyses are available here https://zenodo.org/records/13285406.

4 Stellar activity and false positive detections

Achieving $m\,s^{-1}$ and even $cm\,s^{-1}$ precision in RV measurements is a complex task due to various instrumental and observational limitations, but also due to Stellar activity. The influence of stellar activity on RV measurements is complex and perhaps the most crucial topic in the search for exoplanets. The implications of stellar activity are numerous and cannot be fully discussed in this work. Therefore, for a more detailed yet easy-to-understand overview of the different stellar activity-induced effects on RV data, we recommend Chapters 9 and 10 in (Hatzes, 2019).

Here, we discuss the most prominent astrophysical limitations, which, separately or combined, are the main reason for hampering the firm detection of low-mass exoplanets similar to that of Earth.

4.1 Stellar jitter

A significant source of RV noise originates from astrophysical phenomena within stars, over which astronomers have literally no control. Several intrinsic stellar phenomena contribute to what is known as "RV jitter", with solar-type p-mode oscillations being the dominant process. In the Sun, these p-mode pulsations are attributed to the periodic expansion and contraction of the solar surface, producing small,

correlated RV noise with time scales of approximately 5 minutes. Given the typically sparse cadence of exoplanet surveys, this correlated noise appears as stochastic RV noise. Every star exhibits an "RV jitter" and its amplitude and timescale depend on various factors such as stellar type, age, and radius. For instance, G-type solar stars appear relatively quiet during the MS phase but show a significant increase in jitter as they evolve onto the red giant branch (Kjeldsen and Bedding, 2011).

RV jitter presents a major challenge in exoplanet research, particularly when detecting and characterizing very small exoplanets. It is crucial to account for RV jitter when analyzing radial velocity data to ensure accurate interpretation of any detected signals that could potentially originate from exoplanets. One strategy to mitigate the effects of jitter is to accumulate a large number of RV observations, thereby enhancing the significance of exoplanet signals relative to the RV noise. Although this approach is costly, it is perhaps the only feasible method to detect small Earth-mass planets around solar-type stars. Fortunately, astronomers have developed effective numerical techniques to manage RV jitter. When fitting orbits and estimating uncertainties in orbital parameters, we can include the RV jitter term in quadrature to the total error budget, treating RV jitter as originating from stochastic processes:

$$\sigma_{i,n} = \sqrt{\sigma_i^2 + \sigma_{\text{jitter,n}}^2} \tag{17}$$

Here, for each RV dataset n, we add the RV jitter term $\sigma_{\text{jitter,n}}$ to each i-th uncertainty. It is important to understand that what we call "RV jitter" may, in fact, result from a combination of astrophysical and instrumental noise. Therefore, we adopt different jitter terms for each RV dataset.

Following the prescription of Baluev (2009) of incorporating a parameter term for the stochastic stellar RV jitter for each used RV dataset into the $\ln \mathcal{L}$ function, the log-likelihood function now has the form:

$$\ln \mathcal{L}(\theta) = -\frac{1}{2} \sum_{i=1}^{N} \left[\frac{(v_i - V(t_i; \theta))^2}{\sigma_i^2 + \sigma_{\text{jitter,n}}^2} + \ln \left(\sqrt{2\pi(\sigma_i^2 + \sigma_{\text{jitter,n}}^2)} \right) \right] \tag{18}$$

This inclusion helps obtain a realistic estimation of the RV scatter and ensures the integrity of the derived orbital solutions and estimated parameter uncertainties. High-resolution spectrographs and advanced data processing techniques are crucial in dissecting these contributions to jitter. Ultimately, understanding and correcting for RV jitter is essential for the reliable detection of Earth-like exoplanets.

4.2 Stellar Activity: A Source of False Exoplanet Detections

One significant source of astrophysical noise is induced by stellar rotational modulation, which can severely impact exoplanet detectability. Stars typically rotate over a period of days, and stars similar to the Sun have spots and plages that move across the stellar disk as the star rotates. This phenomenon causes flux variations in the stellar regions they traverse, leading to differences in weight of the blue-shifted and red-shifted part of the stellar disk. These shifts create stellar line asymmetries, which our RV extraction pipelines interpret as Doppler shifts. Since these signals could be periodic, they can mimic the RV signals from exoplanets.

The challenge of distinguishing between signals caused by stellar activity and those due to gravitational influences from exoplanets is significant. Stellar activity can introduce RV variations that are often indistinguishable from those caused by orbiting planets without careful analysis. This complexity is compounded by the effects of the rotation period P_{rot} and its harmonics ($P_{\text{rot}}/2, P_{\text{rot}}/3, \ldots$), which can appear in the RV data depending on the number and arrangement of active regions on the stellar surface. Accurately identifying these signals requires sophisticated techniques like Fourier analysis to parse out the fundamental rotational frequency from its harmonics.

Stellar magnetic activity also plays a crucial role, particularly through phenomena like sunspots, faculae, and flares, which cause localized surface velocity and brightness changes, leading to further complications in RV data analysis. For instance, the ~11-year Solar cycles can induce RV variations with amplitudes and periods similar to those of Jupiter.

Stellar granulation is another significant source of stellar RV jitter, arising from the convective motion within a star's photosphere. This granulation leads to varying RV signals as different parts of the star's surface move relative to each other, contributing to the overall noise level in RV measurements.

Stellar activity and its effects on RV measurements are more pronounced in young stars. These stars, particularly those younger than 1 G yr, exhibit small rotational periods that can closely align with the orbital periods of potential exoplanets, complicating the differentiation between stellar and planetary signals. The magnetic dynamo, which drives this activity, is stronger in younger stars, leading to larger and more numerous active regions. As stars age, their rotation slows, and the dynamo weakens, reducing the size and impact of active regions.

For exoplanet searches, this necessitates focusing on older, slowly rotating stars where activity levels are lower and less likely to interfere with RV measurements. On the other hand, extreme cases such as evolved old stars such as K-giants are suspected to exhibit non-radial pulsations, which can also mimic planets (Hatzes et al., 2018). Techniques such as observing in the near-infrared domain have been proposed to mitigate these issues, as the contrast of dark spots is reduced at these wavelengths. Doppler signals due to orbiting companions are wavelength-independent. Additionally, the use of spectroscopic indicators like the line bisector (Queloz et al., 2001) and the Ca II H&K chromosphere index help in identifying and correcting for activity-related distortions in RV data.

Achieving high precision in RV measurements and confidently confirming the presence of exoplanets amidst the noise of stellar activity is an ongoing challenge. One effective strategy is to densely sample and average data over periods comparable to the star's rotation period. This approach helps enhance precision and manage the influence of stellar activity. By understanding and accounting for these factors, researchers can improve the accuracy of exoplanet detection and avoid mistakenly interpreting stellar noise as planetary signals.

5 The future

Technological advancements in spectroscopy aim to develop highly stable, high-resolution spectrographs capable of measuring RVs down to 10 cm s^{-1}, in the near future. The primary goal of reaching such extreme RV precision is to enable the identification of Earth-like exoplanets in the HZ around stars similar to our Sun. Notable projects in this ambitious field include "The Terra Hunting Experiment" (Thompson et al., 2016), the EXtreme PREcision Spectrometer (EXPRES, Jurgenson et al., 2016), and the "Second Earth Initiative Spectrograph (2ES)" (Buchhave et al. in prep.). These future Doppler surveys are designed to discover Earth-mass exoplanets with orbital periods close to one year around nearby Sun-like stars. The Échelle instruments being developed for these surveys will utilize significantly improved versions of existing instruments like the HARPS and MAROON-X spectrographs, which are already capable of reaching precision well below 1 m s^{-1}, will be installed on 3-meter class telescopes. These surveys aim to collect numerous RV measurements in an automated fashion for a relatively small sample of nearby Sun-like stars over a decade-long period.

However, achieving a precision of 10 cm s^{-1} is only the first major milestone. A deeper understanding of stellar activity is needed, and the exoplanet field is actively working in this direction. Fortunately, large-scale insights into stellar activity are recorded in the spectra, and future high-resolution spectrographs will certainly help tackle the challenge of stellar noise. By continuously monitoring stars over many years on a high cadence, researchers aim to overcome instrumental and stellar activity signals, providing unprecedented insights into the presence of terrestrial planets in our solar neighborhood.

Another important aspect of RV detection is the continuation of RV surveys, which, by increasing the temporal baseline of the RVs, will reveal the population of cold Jovian analogs located at orbital distances between 5-20 au, similar to the giants in our Solar System. This exoplanet demographics region is still to be explored (see Fig.3).

In terms of high-resolution, high-SNR spectra, some of these spectrographs, which are planned to be utilized on 8-meter class telescopes or future extremely large telescopes (ELTs), would be ideal for exoplanet atmosphere characterization of rocky planets using transmission spectroscopy. Apart from the ongoing efforts in recording ultra-precise RV measurements and transmission and emission spectroscopy using ESPRESSO (Pepe et al., 2021) at the VLT in Chile, another notable project must be mentioned. The ArmazoNes high Dispersion Échelle Spectrograph (ANDES) is a high-resolution optical and near-infrared spectrograph being developed for the Extremely Large Telescope (ELT). ANDES is expected to revolutionize exoplanet science by enabling the detection of bio-signatures in exoplanet atmospheres and providing detailed observations of planetary systems (Palle et al., 2023).

The increased RV sensitivity of future spectrographs, combined with existing ones, will enhance the integration of the RV method with other exoplanet detection techniques, such as transit photometry, direct imaging, and forthcoming data from Gaia DR4. The RV method will continue to be vital for characterizing exoplanets, whether used alone or in combination with other techniques.

The potential deployment of space-based RV observatories could revolutionize the method, though currently, this idea is seen as too expensive and technically impractical. The absence of atmospheric disturbances in space would enhance data accuracy and sensitivity. However, deploying high-resolution, high-precision Échelle spectrographs and managing their complex data collection from space presents significant challenges and risks.

Ground-based high-resolution spectroscopy will continue to play a crucial role in characterizing exoplanet atmospheres. As detection capabilities improve, so will the ability to characterize the atmospheres of smaller, Earth-like planets. This progress will be enhanced by combining RV data with that from direct imaging missions, facilitating detailed studies of the climates and chemical compositions of exoplanet atmospheres.

Over the next thirty years, the RV Doppler method will likely enhance its existing capabilities and expand into new realms of astronomical inquiry. Our understanding of the Universe and our place within it will deepen, marking an exciting era of exoplanet discoveries and the characterization of their physical properties.

6 Conclusion

The stellar RV Doppler method has remained an invaluable asset in the arena of exoplanet discovery and research. It has made a giant leap in understanding the universe other than our solar system. RV thus remains a cornerstone technique in the detection of exoplanets and precise measurements of their masses. Constant improvement in spectrographic technologies and enhancement in data analytic methodologies is increasing both sensitivity and accuracy in RV measurements.

In that sense, the integration of the RV data with observation data acquired from other methods, such as transit and astrometric stellar measurements, can fill in missing information about planetary compositions and orbits and give us a detailed and complete view of planetary systems. However, challenges remain, particularly in detecting Earth-like planets due to the subtle signals they produce. The evolution of high-precision spectrographs and advanced statistical techniques has been crucial in overcoming these hurdles and enhancing the sensitivity and accuracy of radial velocity measurements. These technological and methodological advancements are driving a new era in exoplanet

discovery, where the detection of Earth analogs around Sun-like stars becomes increasingly feasible, promising profound implications for our understanding of planetary systems across the galaxy. As such, Doppler surveys continue to play a critical role in the field of exoplanet research, shaping future explorations and studies aimed at uncovering the diversity of planets in our Galaxy.

In that sense, the integration of the RV data with observation data from other methods such as transit and astrometric stellar measurements can complete observations about planetary compositions and orbits, make them complementary, and give us a detailed view of planetary systems. The RV method is bound to bring even bigger discoveries in the future, with improved instruments and techniques, including the detection of Earth twins at Sun-like stars. The RV method, therefore, remains a fundamental tool of exoplanet science, one needed both in the relentless quest for new worlds and in their later detailed characterization.

Acknowledgments

See Also: Many excellent reviews and textbooks are available on the Doppler method for detecting exoplanets. However, I highly recommend *The Doppler Method for the Detection of Exoplanets* by Artie Hatzes (Hatzes, 2019), which served as my primary guide reference while writing this chapter.

References

Anglada-Escudé G, Amado PJ, Barnes J, Berdiñas ZM, Butler RP, Coleman GAL, de La Cueva I, Dreizler S, Endl M, Giesers B, Jeffers SV, Jenkins JS, Jones HRA, Kiraga M, Kürster M, López-González MJ, Marvin CJ, Morales N, Morin J, Nelson RP, Ortiz JL, Ofir A, Paardekooper SJ, Reiners A, Rodríguez E, Rodríguez-López C, Sarmiento LF, Strachan JP, Tsapras Y, Tuomi M and Zechmeister M (2016), Aug. A terrestrial planet candidate in a temperate orbit around Proxima Centauri. *Nature* 536 (7617): 437–440. doi:10.1038/nature19106. 1609.03449.

Baluev RV (2009), Mar. Accounting for velocity jitter in planet search surveys. *MNRAS* 393: 969–978. doi:10.1111/j.1365-2966.2008.14217.x. 0712.3862.

Baranne A, Queloz D, Mayor M, Adrianzyk G, Knispel G, Kohler D, Lacroix D, Meunier JP, Rimbaud G and Vin A (1996). Elodie: A spectrograph for accurate radial velocity measurements. *Astronomy and Astrophysics Supplement Series* 119 (2): 373–390.

Borucki WJ, Koch D, Basri G, Batalha N, Brown T, Caldwell D, Caldwell J, Christensen-Dalsgaard J, Cochran WD, DeVore E, Dunham EW, Dupree AK, Gautier TN, Geary JC, Gilliland R, Gould A, Howell SB, Jenkins JM, Kondo Y, Latham DW, Marcy GW, Meibom S, Kjeldsen H, Lissauer JJ, Monet DG, Morrison D, Sasselov D, Tarter J, Boss A, Brownlee D, Owen T, Buzasi D, Charbonneau D, Doyle L, Fortney J, Ford EB, Holman MJ, Seager S, Steffen JH, Welsh WF, Rowe J, Anderson H, Buchhave L, Ciardi D, Walkowicz L, Sherry W, Horch E, Isaacson H, Everett ME, Fischer D, Torres G, Johnson JA, Endl M, MacQueen P, Bryson ST, Dotson J, Haas M, Kolodziejczak J, Van Cleve J, Chandrasekaran H, Twicken JD, Quintana EV, Clarke BD, Allen C, Li J, Wu H, Tenenbaum P, Verner E, Bruhweiler F, Barnes J and Prsa A (2010), Feb. Kepler Planet-Detection Mission: Introduction and First Results. *Science* 327 (5968): 977. doi:10.1126/science.1185402.

Butler RP, Marcy GW, Williams E, McCarthy C, Dosanjh P and Vogt SS (1996), Jun. Attaining Doppler Precision of 3 M s-1. *PASP* 108: 500. doi:10.1086/133755.

Butler RP, Vogt SS, Laughlin G, Burt JA, Rivera EJ, Tuomi M, Teske J, Arriagada P, Diaz M, Holden B and Keiser S (2017), May. The LCES HIRES/Keck Precision Radial Velocity Exoplanet Survey. *AJ* 153, 208. doi:10.3847/1538-3881/aa66ca. 1702.03571.

Campbell WW and Moore JH (1926), Aug. The Elements of the Solar Motion Derived from Stars Of Visual Magnitude Brighter than 5.51 (Abstarct). *PASP* 38 (224): 255. doi:10.1086/123600.

Campbell B and Walker GAH (1979), Aug. Precision radial velocities with an absorption cell. *PASP* 91: 540–545. doi:10.1086/130535.

Campbell B, Walker GAH and Yang S (1988), Jan., A Search for Planetary Mass Companions to Nearby Stars, Marx G, (Ed.), IAU Colloq. 99: Bioastronomy - The Next Steps, Astrophysics and Space Science Library, 144, 83–90.

Charbonneau D, Brown TM, Latham DW and Mayor M (2000), Jan. Detection of Planetary Transits Across a Sun-like Star. *ApJ* 529 (1): L45–L48. doi:10.1086/312457. astro-ph/9911436.

Damasso M, Del Sordo F, Anglada-Escudé G, Giacobbe P, Sozzetti A, Morbidelli A, Pojmanski G, Barbato D, Butler RP, Jones HRA, Hambsch FJ, Jenkins JS, López-González MJ, Morales N, Peña Rojas PA, Rodríguez-López C, Rodríguez E, Amado PJ, Anglada G, Feng F and Gómez JF (2020), Jan. A low-mass planet candidate orbiting Proxima Centauri at a distance of 1.5 AU. *Science Advances* 6 (3): eaax7467. doi:10.1126/sciadv.aax7467.

Eversberg T and Vollmann K (2015). Spectroscopic Instrumentation: Fundamentals and Guidelines for Astronomers. doi:10.1007/978-3-662-44535-8.

Faria JP, Suárez Mascareño A, Figueira P, Silva AM, Damasso M, Demangeon O, Pepe F, Santos NC, Rebolo R, Cristiani S, Adibekyan V, Alibert Y, Allart R, Barros SCC, Cabral A, D'Odorico V, Di Marcantonio P, Dumusque X, Ehrenreich D, González Hernández JI, Hara N, Lillo-Box J, Lo Curto G, Lovis C, Martins CJAP, Mégevand D, Mehner A, Micela G, Molaro P, Nunes NJ, Pallé E, Poretti E, Sousa SG, Sozzetti A, Tabernero H, Udry S and Zapatero Osorio MR (2022), Feb. A candidate short-period sub-Earth orbiting Proxima Centauri. *A&A* 658, A115. doi:10.1051/0004-6361/202142337. 2202.05188.

Fischer DA and Valenti J (2005), Apr. The Planet-Metallicity Correlation. *ApJ* 622 (2): 1102–1117. doi:10.1086/428383.

Ford EB and Rasio FA (2008), Oct. Origins of Eccentric Extrasolar Planets: Testing the Planet-Planet Scattering Model. *ApJ* 686 (1): 621–636. doi:10.1086/590926. astro-ph/0703163.

Gaudi BS (2012), Sep. Microlensing Surveys for Exoplanets. *ARA&A* 50: 411–453. doi:10.1146/annurev-astro-081811-125518.

Golovin A, Reffert S, Just A, Jordan S, Vani A and Jahreiß H (2023), Feb. The Fifth Catalogue of Nearby Stars (CNS5). *A&A* 670, A19. doi:

10.1051/0004-6361/202244250. 2211.01449.

Griffin RF (1967), Jan., Photoelectric Measurement of Radial Velocities, Batten AH and Heard JF, (Eds.), Determination of Radial Velocities and their Applications, 30, pp. 3.

Griffin RF (1978), Feb. Spectroscopic binary orbits from photoelectric radial velocities. Paper 18: HR 6388. *The Observatory* 98: 14–18.

Hatzes AP (2019). The Doppler Method for the Detection of Exoplanets. doi:10.1088/2514-3433/ab46a3.

Hatzes AP and Cochran WD (1993), Aug. Long-Period Radial Velocity Variations in Three K Giants. *ApJ* 413: 339. doi:10.1086/173002.

Hatzes AP, Cochran WD, Endl M, McArthur B, Paulson DB, Walker GAH, Campbell B and Yang S (2003), Dec. A Planetary Companion to γ Cephei A. *ApJ* 599 (2): 1383–1394. doi:10.1086/379281. astro-ph/0305110.

Hatzes AP, Endl M, Cochran WD, MacQueen PJ, Han I, Lee BC, Kim KM, Mkrtichian D, Döllinger M, Hartmann M, Karjalainen M and Dreizler S (2018), Mar. The Radial Velocity Variability of the K-giant γ Draconis: Stellar Variability Masquerading as a Planet. *AJ* 155 (3), 120. doi:10.3847/1538-3881/aaa8e1. 1801.05239.

Jurgenson C, Fischer D, McCracken T, Sawyer D, Szymkowiak A, Davis A, Muller G and Santoro F (2016), Aug., EXPRES: a next generation RV spectrograph in the search for earth-like worlds, Evans CJ, Simard L and Takami H, (Eds.), Ground-based and Airborne Instrumentation for Astronomy VI, Society of Photo-Optical Instrumentation Engineers (SPIE) Conference Series, 9908, pp. 99086T, 1606.04413.

Kjeldsen H and Bedding TR (2011), May. Amplitudes of solar-like oscillations: a new scaling relation. *A&A* 529, L8. doi:10.1051/0004-6361/201116789. 1104.1659.

Latham DW, Mazeh T, Stefanik RP, Mayor M and Burki G (1989), May. The unseen companion of HD114762: a probable brown dwarf. *Nature* 339 (6219): 38–40. doi:10.1038/339038a0.

Lee MH and Peale SJ (2002), Mar. Dynamics and Origin of the 2:1 Orbital Resonances of the GJ 876 Planets. *ApJ* 567: 596–609. doi:10.1086/338504.

Lo Curto G, Pepe F, Fleury M, Hughes I, Schnell R, Wimmer V, Fuerte Rodriguez PA, Silber A, Saviane I, Lovis C, Sosnowska D, Dumusque X, Jakob G and Accardo M (2024), Mar. HARPS at 20: Evolving Through Continuous Improvements. *The Messenger* 192: 38–40. doi:10.18727/0722-6691/5354.

Marcy GW and Butler RP (1992), Apr. Precision radial velocities with an iodine absorption cell. *PASP* 104: 270–277. doi:10.1086/132989.

Marcy GW, Butler RP, Williams E, Bildsten L, Graham JR, Ghez AM and Jernigan JG (1997), May. The Planet around 51 Pegasi. *ApJ* 481 (2): 926–935. doi:10.1086/304088.

Marois C, Macintosh B, Barman T, Zuckerman B, Song I, Patience J, Lafrenière D and Doyon R (2008), Nov. Direct Imaging of Multiple Planets Orbiting the Star HR 8799. *Science* 322 (5906): 1348. doi:10.1126/science.1166585. 0811.2606.

Mayor M and Queloz D (1995), Nov. A Jupiter-mass companion to a solar-type star. *Nature* 378 (6555): 355–359. doi:10.1038/378355a0.

Mayor M, Pepe F, Queloz D, Bouchy F, Rupprecht G, Lo Curto G, Avila G, Benz W, Bertaux JL, Bonfils X, Dall T, Dekker H, Delabre B, Eckert W, Fleury M, Gilliotte A, Gojak D, Guzman JC, Kohler D, Lizon JL, Longinotti A, Lovis C, Megevand D, Pasquini L, Reyes J, Sivan JP, Sosnowska D, Soto R, Udry S, van Kesteren A, Weber L and Weilenmann U (2003), Dec. Setting New Standards with HARPS. *The Messenger* 114: 20–24.

Nelder JA and Mead R (1965). A simplex method for function minimization. *Computer Journal* 7: 308–313.

Palle E, Biazzo K, Bolmont E, Molliere P, Poppenhaeger K, Birkby J, Brogi M, Chauvin G, Chiavassa A, Hoeijmakers J, Lellouch E, Lovis C, Maiolino R, Nortmann L, Parviainen H, Pino L, Turbet M, Wender J, Albrecht S, Antoniucci S, Barros SC, Beaudoin A, Benneke B, Boisse I, Bonomo AS, Borsa F, Brandeker A, Brandner W, Buchhave LA, Cheffot AL, Deborde R, Debras F, Doyon R, Di Marcantonio P, Giacobbe P, Gonzalez Hernandez JI, Helled R, Kreidberg L, Machado P, Maldonado J, Marconi A, Canto Martins BL, Miceli A, Mordasini C, N'Diaye M, Niedzielski A, Nisini B, Origlia L, Peroux C, Pietrow AGM, Pinna E, Rauscher E, Reffert S, Rousselot P, Sanna N, Simonnin A, Suarez Mascareno A, Zanutta A and Zechmeister M (2023), Nov. Ground-breaking Exoplanet Science with the ANDES spectrograph at the ELT. *arXiv e-prints* , arXiv:2311.17075doi:10.48550/arXiv.2311.17075. 2311.17075.

Pepe F, Cristiani S, Rebolo R, Santos NC, Dekker H, Cabral A, Di Marcantonio P, Figueira P, Lo Curto G, Lovis C, Mayor M, Mégevand D, Molaro P, Riva M, Zapatero Osorio MR, Amate M, Manescau A, Pasquini L, Zerbi FM, Adibekyan V, Abreu M, Affolter M, Alibert Y, Aliverti M, Allart R, Allende Prieto C, Álvarez D, Alves D, Avila G, Baldini V, Bandy T, Barros SCC, Benz W, Bianco A, Borsa F, Bourrier V, Bouchy F, Broeg C, Calderone G, Cirami R, Coelho J, Conconi P, Coretti I, Cumani C, Cupani G, D'Odorico V, Damasso M, Deiries S, Delabre B, Demangeon ODS, Dumusque X, Ehrenreich D, Faria JP, Fragoso A, Genolet L, Genoni M, Génova Santos R, González Hernández JI, Hughes I, Iwert O, Kerber F, Knudstrup J, Landoni M, Lavie B, Lillo-Box J, Lizon JL, Maire C, Martins CJAP, Mehner A, Micela G, Modigliani A, Monteiro MA, Monteiro MJPFG, Moschetti M, Murphy MT, Nunes N, Oggioni L, Oliveira A, Oshagh M, Pallé E, Pariani G, Poretti E, Rasilla JL, Rebordão J, Redaelli EM, Santana Tschudi S, Santin P, Santos P, Ségransan D, Schmidt TM, Segovia A, Sosnowska D, Sozzetti A, Sousa SG, Spanò P, Suárez Mascareño A, Tabernero H, Tenegi F, Udry S and Zanutta A (2021), Jan. ESPRESSO at VLT. On-sky performance and first results. *A&A* 645, A96. doi:10.1051/0004-6361/202038306. 2010.00316.

Queloz D, Henry GW, Sivan JP, Baliunas SL, Beuzit JL, Donahue RA, Mayor M, Naef D, Perrier C and Udry S (2001), Nov. No planet for HD 166435. *A&A* 379 (1): 279–287. ISSN 0004-6361, 1432-0756. doi:10.1051/0004-6361:20011308. http://www.edpsciences.org/10.1051/0004-6361:20011308.

Reffert S, Bergmann C, Quirrenbach A, Trifonov T and Künstler A (2015), Feb. Precise radial velocities of giant stars. VII. Occurrence rate of giant extrasolar planets as a function of mass and metallicity. *A&A* 574, A116. doi:10.1051/0004-6361/201322360. 1412.4634.

Reiners A, Ribas I, Zechmeister M, Caballero JA, Trifonov T, Dreizler S, Morales JC, Tal-Or L, Lafarga M, Quirrenbach A, Amado PJ, Kaminski A, Jeffers SV, Aceituno J, Béjar VJS, Guàrdia J, Guenther EW, Hagen HJ, Montes D, Passegger VM, Seifert W, Schweitzer A, Cortés-Contreras M, Abril M, Alonso-Floriano FJ, Ammler-von Eiff M, Antona R, Anglada-Escudé G, Anwand-Heerwart H, Arroyo-Torres B, Azzaro M, Baroch D, Barrado D, Bauer FF, Becerril S, Benítez D, Berdiñas ZM, Bergond G, Blümcke M, Brinkmöller M, del Burgo C, Cano J, Cárdenas Vázquez MC, Casal E, Cifuentes C, Claret A, Colomé J, Czesla S, Díez-Alonso E, Feiz C, Fernández M, Ferro IM, Fuhrmeister B, Galadí-Enríquez D, Garcia-Piquer A, García Vargas ML, Gesa L, Gómez Galera V, González Hernández JI, González-Peinado R, Grözinger U, Grohnert S, Guijarro A, de Guindos E, Gutiérrez-Soto J, Hatzes AP, Hauschildt PH, Hedrosa RP, Helmling J, Henning T, Hermelo I, Hernández Arabí R, Hernández Castaño L, Hernández Hernando F, Herrero E, Huber A, Huke P, Johnson EN, de Juan E, Kim M, Klein R, Klüter J, Klutsch A, Kürster M, Labarga F, Lamert A, Lampón M, Lara LM, Laun W, Lemke U, Lenzen R, Launhardt R, López del Fresno M, López-González MJ, López-Puertas M, López Salas JF, López-Santiago J, Luque R, Magán Madinabeitia H, Mall U, Mancini L, Mand el H, Marfil E, Marín Molina JA, Maroto Fernández D, Martín EL, Martín-Ruiz S, Marvin CJ, Mathar RJ, Mirabet E, Moreno-Raya ME, Moya A, Mundt R, Nagel E, Naranjo V, Nortmann L, Nowak G, Ofir A, Oreiro R, Pallé E, Panduro J, Pascual J, Pavlov A, Pedraz S, Pérez-Calpena A, Pérez Medialdea D, Perger M, Perryman MAC, Pluto M, Rabaza O, Ramón A, Rebolo R, Redondo P, Reffert S, Reinhart S, Rhode P, Rix HW, Rodler F, Rodríguez E, Rodríguez-López C, Rodríguez Trinidad A, Rohloff RR, Rosich A, Sadegi S, Sánchez-Blanco E, Sánchez Carrasco MA, Sánchez-López A, Sanz-Forcada J, Sarkis P, Sarmiento LF, Schäfer S, Schmitt JHMM, Schiller J, Schöfer P, Solano E, Stahl O, Strachan JBP, Stürmer J, Suárez JC, Tabernero HM, Tala M, Tulloch SM, Ulbrich RG, Veredas G, Vico Linares JI, Vilardell F, Wagner K, Winkler J, Wolthoff V, Xu W, Yan F and Zapatero Osorio MR (2018), Jan. The CARMENES search for exoplanets around M dwarfs. HD147379 b: A nearby Neptune in the temperate

zone of an early-M dwarf. *A&A* 609, L5. doi:10.1051/0004-6361/201732165. 1712.05797.

Ricker GR, Winn JN, Vanderspek R, Latham DW, Bakos GÁ, Bean JL, Berta-Thompson ZK, Brown TM, Buchhave L, Butler NR, Butler RP, Chaplin WJ, Charbonneau D, Christensen-Dalsgaard J, Clampin M, Deming D, Doty J, De Lee N, Dressing C, Dunham EW, Endl M, Fressin F, Ge J, Henning T, Holman MJ, Howard AW, Ida S, Jenkins JM, Jernigan G, Johnson JA, Kaltenegger L, Kawai N, Kjeldsen H, Laughlin G, Levine AM, Lin D, Lissauer JJ, MacQueen P, Marcy G, McCullough PR, Morton TD, Narita N, Paegert M, Palle E, Pepe F, Pepper J, Quirrenbach A, Rinehart SA, Sasselov D, Sato B, Seager S, Sozzetti A, Stassun KG, Sullivan P, Szentgyorgyi A, Torres G, Udry S and Villasenor J (2015), Jan. Transiting Exoplanet Survey Satellite (TESS). *Journal of Astronomical Telescopes, Instruments, and Systems* 1 (1), 014003. doi:10.1117/1.JATIS.1.1.014003.

Sabotta S, Schlecker M, Chaturvedi P, Guenther EW, Muñoz Rodríguez I, Muñoz Sánchez JC, Caballero JA, Shan Y, Reffert S, Ribas I, Reiners A, Hatzes AP, Amado PJ, Klahr H, Morales JC, Quirrenbach A, Henning T, Dreizler S, Pallé E, Perger M, Azzaro M, Jeffers SV, Kaminski A, Kürster M, Lafarga M, Montes D, Passegger VM and Zechmeister M (2021), Sep. The CARMENES search for exoplanets around M dwarfs. Planet occurrence rates from a subsample of 71 stars. *A&A* 653, A114. doi:10.1051/0004-6361/202140968. 2107.03802.

Thompson SJ, Queloz D, Baraffe I, Brake M, Dolgopolov A, Fisher M, Fleury M, Geelhoed J, Hall R, González Hernández JI, ter Horst R, Kragt J, Navarro R, Naylor T, Pepe F, Piskunov N, Rebolo R, Sander L, Ségransan D, Seneta E, Sing D, Snellen I, Snik F, Spronck J, Stempels E, Sun X, Santana Tschudi S and Young J (2016), Aug., HARPS3 for a roboticized Isaac Newton Telescope, Evans CJ, Simard L and Takami H, (Eds.), Ground-based and Airborne Instrumentation for Astronomy VI, Society of Photo-Optical Instrumentation Engineers (SPIE) Conference Series, 9908, pp. 99086F, 1608.04611.

Vogt SS (1987), Nov. The Lick Observatory Hamilton echelle spectrometer. *PASP* 99: 1214–1228. doi:10.1086/132107.

Walker GAH, Bohlender DA, Walker AR, Irwin AW, Yang SLS and Larson A (1992), Sep. Gamma Cephei: Rotation or Planetary Companion? *ApJ* 396: L91. doi:10.1086/186524.

Wolthoff V, Reffert S, Quirrenbach A, Jones MI, Wittenmyer RA and Jenkins JS (2022), May. Precise radial velocities of giant stars. XVI. Planet occurrence rates from the combined analysis of the Lick, EXPRESS, and PPPS giant star surveys. *A&A* 661, A63. doi:10.1051/0004-6361/202142501. 2202.12800.

Zechmeister M and Kürster M (2009), Mar. The generalised Lomb-Scargle periodogram. A new formalism for the floating-mean and Keplerian periodograms. *A&A* 496: 577–584. doi:10.1051/0004-6361:200811296. 0901.2573.